# AUTHOR QUERIES

# AUTHOR PLEASE ANSWER ALL QUERIES

**PLEASE NOTE: We cannot accept new source files as corrections for your paper. If possible, please annotate the PDF proof we have sent you with your corrections and upload it via the Author Gateway. Alternatively, you may send us your corrections in list format. You may also upload revised graphics via the Author Gateway.**

**Carefully check the page proofs (and coordinate with all authors); additional changes or updates WILL NOT be accepted after the article is published online/print in its final form. Please check author names and affiliations, funding, as well as the overall article for any errors prior to sending in your author proof corrections. Your article has been peer reviewed, accepted as final, and sent in to IEEE. No text changes have been made to the main part of the article as dictated by the editorial level of service for your publication.**

AQ1: Please confirm or add details for any funding or financial support for the research of this article.

AQ2: References [13] and [16] were the same in your originally submitted manuscript, so Reference [16] has been deleted and the remaining references (and their in text citations) have been renumbered. Please check and confirm that they are correct as set.

# An Earth Fault Diagnosis Method Based on Online Dynamically Calculated Thresholds for Resonant Ground Systems

Jiahao Lin, Student Member, IEEE, Moufa Guo, Member, IEEE, Qiteng Hong, Senior Member, IEEE, and Run Jiang, Student Member, IEEE

***Abstract*—The primary problem of distribution system protection is single-line-to-ground (SLG) fault, particularly in networks with distributed generators (DGs), where asymmetrical phase sequence components caused by SLG faults may lead to system instability. Currently, the location and suppression methods of SLG faults are based on reliable fault diagnosis. Therefore, considering the imbalance of line parameters, this paper analyzes the component fault characteristics of zero-sequence voltage (ZSV), and proposes a threshold-online-calculating-based SLG fault diagnosis method, which includes fault detection, fault occurrence moment capture and fault nature estimation. Firstly, the ZSV is measured in real time by the designed feeder terminal unit (FTU), which is embedded with the proposed SLG fault diagnosis method. Secondly, the ZSV signal is decomposed by the Mallat algorithm, and the fault diagnosis thresholds are calculated through the maximum margin hyperplane, which is used for fault detection and fault nature estimation. Finally, the fault occurrence moment sensing is captured by variational mode decomposition (VMD) and its Teager Energy Operator (TEO). The proposed SLG fault diagnosis method has been tested in simulation and physical experiments in a 10kV system, the effectiveness and feasibility have been validated.**

***Index Terms*—Distribution network, single-line-to-ground fault, fault diagnosis method, fault occurrence moment capture, fault nature estimation.**

## I. INTRODUCTION

THE NEUTRAL point of medium-voltage (MV) power ... emsaretypicallyearthedvia an arc ... suppression coil (ASC) in Europe, Africa, Asia and some parts of North America [1], [2], which is called resonant ground system. The SLG faults account for more than 80% of distribution network line faults, and the ASC is utilized to suppress the fault current [3], [4]. However, during SLG faults, ASC will change the fault characteristics, challenging fault detection and fault location, especially for high impedance faults (HIF) [5], [6]. Furthermore, if the ground fault is accompanied by intermittent arcing, it will lead to arc overvoltage, which could risk the insulation of the line being damaged. In addition, ASC cannot fully suppress the active component and high-frequency harmonics component, which may cause accidents such as fire and large-scale power outages [7].

In addition, smart power distribution systems are gradually being implemented driven by the widespread integration of distributed generators (DGs), and the development of sensing and communication technologies [8]. The smart power distribution systems can realize multi-energy flow synergy, namely "electricity-gas-heat". By combining existing sensing and communication technologies, the information interaction of "source-network-load" can be realized. It helps to improve the self-diagnosis capability which is a pivotal characteristic of the smart power distribution system [9], [10]. When an SLG fault occurs, determining the faulty feeder or faulty section is necessary [11],[12]. Additionally, in a resonant ground system with an active arc suppression device, rapid initiation of the arc suppression device after SLG faults is important [13], [14]. The traditional method mainly uses a ZSV threshold (typically set at 15% of the phase voltage) as the fault detection criterion [11],[15]. In a neutral ungrounded system, the amplitude of ZSV may not satisfy traditional fault detection criteria in the case of HIFs. Furthermore, the distribution systems ... amplitude of ZSV rises slowly in resonant ground systems, which satisfies the fault detection criterion only after several cycles from the fault occurrence moment. Most of the existing methods extract fault transient features based on the moment when the fault is detected, which may lead to inaccurate transient feature extraction and affect the accuracy of faulty feeder and faulty section identification. Consequently, the rapid detection of SLG faults and accurate capture of fault occurrence moment are crucial.

In recent years, numerous methods for SLG fault detection have been proposed, such as those based on signal processing technology and artificial intelligence (AI). Among them, the

AQ1

Manuscript received 21 March 2023; revised 3 September 2023 and 2 November 2023; accepted 16 December 2023. This work was supported in part by the National Natural Science Foundation of China under Grant 51677030. Paper no. TSG-00419-2023.

Jiahao Lin, Moufa Guo, and Run Jiang are with the College of Electrical Engineering and Automation and the Fujian Key Laboratory of New Energy Generation and Power Conversion, Fuzhou University, Fuzhou 350108, China (e-mail: jh_fd5678@163.com; gmf@fzu.edu.cn; 210110002@fzu.edu.cn).

Qiteng Hong is with the Department of Electronic and Electrical Engineering, University of Strathclyde, G1 1XW Glasgow, U.K. (e-mail: q.hong@strath.ac.uk).

Color versions of one or more figures in this article are available at https://doi.org/10.1109/TSG.2023.3346453.

Digital Object Identifier 10.1109/TSG.2023.3346453

1949-3053



(Corresponding author: Moufa Guo.)

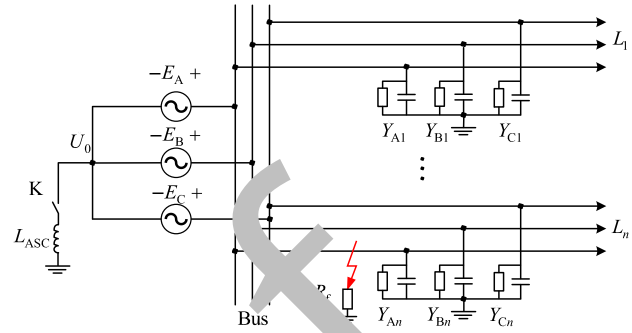


Reference [16] detects HIFs by summing the periodic variation ofZSV.Themethodishighlyfeasible,butthedetectiontime is long. In [17], mathematical morphology is utilized as the detection method for HIFs. This method is sensitive to the variation of ZSV but is susceptible to non-fault disturbances. Reference [18] introduces the SLG fault detection method that calculates the input impedance and locates the fault position by the impulse injection in power line communication, but it is suitable only for HIFs. The time-frequency analysis methods retain the time-frequency characteristics of the waveform. This method is widely used because it can extract more transient character- Fig. 1. SLG fault of resonant ground system. istics of SLG faults. The time-frequency analysis algorithm mainly consists of short-time Fourier Transform (STFT) [19], Hilbert-Huang transform (HHT) [20], wavelet transform algorithm. Finally, the criteria for fault nature estimation are (WT) [21], [22], variational mode decomposition (VMD) [23], defined. The effectiveness and feasibility of the proposed SLG empirical mode decomposition (EMD) [24], etc. In [21] faultdiagnosismethodareverifiedbysimulation,experimental and [25], Guo et al. utilized the Mallat algorithm to simplify and field data. wavelet transform and realized the rapid detection of SLG The remainder of the paper is organized as follows. faults. However, the determination of the threshold coefficient Section II analyzes the SLG fault characteristics of ZSV relies on empirical knowledge. The applicability is limited under different conditions. In Section III, the fault diagnosis with high sensitivity to non-fault disturbances, which have method is proposed, including fault detection, fault occurrence a high risk to cause mal-detection of faults. In [13], a HIF moment capture and fault nature estimation. In Section IV, the detection method based on empirical wavelet transform (EWT) proposed method is verified by simulation data. In Section V, is proposed, which realizes the adaptive selection of fault theproposedmethodisverifiedbyexperimentalandfielddata. characteristic frequency bands. However, the methods based Section VI draws the conclusions. on modal decomposition are computationally time-consuming, resultinginalongtimeforfaultdetection. II.ANALYSISOFZERO-SEQUENCEVOLTAGE AI-basedmethodsfindextensiveapplicationinfaultdiag- CHARACTERISTICS nosis and location because of their powerful data processing

*A. The ZSV Analysis of SLG Fault*

capabilities [26], [27], [28]. Unlike traditional methods, AI-basedmethodsdonotrequirespecificthresholdstobedefined. 1)*SLGfaultoccurs:*Fig.1illustratesasimplifiedresonant After the AI algorithms are trained by sample data, they can ground system, assuming that the SLG fault occurs on phase automatically calculate the classification boundary. However, A of *Ln*. AI-based fault detection methods typically require a substan- The ZSV can be represented as tialvolumeofhistoricaldataforlearningandtraining,which $U$

$$\dot{}0 = U\dot{}A - \dot{E}\dot{}A \quad (1)$$

presents a significant challenge, as the actual fault data are often limited and difficult to collect. Without sufficient realistic where $U\dot{}$ is the phase-to-ground voltage of the faulty phase, iningdata,itwillle $\dot{E}\dot{}A$traadtooverfittingandweakgeneralization$A$isthesourcevoltageofthefaultyphase.

abilityofAI-basedmethods. DuringanSLGfault,thefaultcurrentflowstothebus In actual distribution network, the relay protection systems through the fault point. In resonant ground systems, the fault are required to isolate permanent faults quickly. Therefore, current can be expressed as the rapid detection of SLG faults and the estimation of

$$()1\text{thefaultnatureareimportant.However,theexistingfault}\dot{I}\dot{}f \approx -U\dot{}0 j\omega C + G - (2)$$

detectionmethodsmostlyfocusontheidentificationofHIF, $j\omega L$ASC

ignoring some key issues, such as the speed of fault detection, where $C$ is the total earth capacitance of resonant ground the accurate estimation of fault nature and the impact of system, $G$ is the total earth conductance, and $L$ASC is the unbalancedlineparameters. inductanceofASC.Ingeneral,topreventtheoccurrenceof

Therefore, this paper proposes an SLG fault diagnosis resonance overvoltage, the detuning degree of pre-tuned ASC method based on online dynamically calculated thresholds, istypicallyestablishedat5%[29].Underthenormalfrequency which is capable of detecting faults rapidly, capturing the f0, it can be approximately considered that the inductive occurrence moment of SLG faults and estimating the fault reactance of ASC is equal to the capacitive impedance of total nature. Firstly, when SLG faults occur or disappear under the earth capacitance. With the frequency increasing, the earth condition of unbalanced line parameters, the characteristics of capacitive impedance decreases, and the inductive reactance of ZSV are analyzed. Then, the appropriate thresholds of SLG ASC increases. At the early stage of SLG fault, the dominant fault occurrence and disappearance can be calculated in real frequency of the system (f1) is typically several times f0, thus time by the maximum margin hyperplane. At the same time, the system is seen as capacitive [11]. During the transient the fault occurrence moment can be captured by VMD-TEO process, the relationship between the inductive reactance of

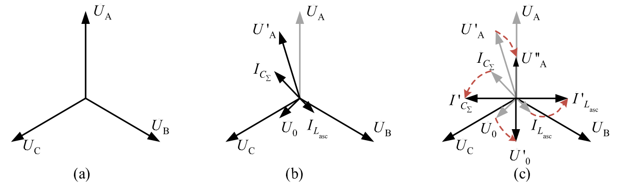


Fig.2. Therelationshipbetweenthree-phasevoltageandZSV:(a)Under normal conditions, (b) SLG fault transient process, (c) SLG fault steady state process.

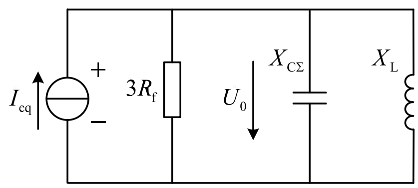


Fig. 3. The equivalent zero-sequence circuit.

ASC and the capacitive impedance of total earth capacitance can be expressed as

()121ωLLASC≈=CC ω1 0 ω 0ASC ω1 ω0ω0 Σ ω 1 ω1 Σ
1 ( ω ) = f21 f01 . ω 0
ω C Σ (3)

It can be seen that the ratio between inductance from the ASC and the phase-to-ground capacitance from the network is$(f1/f)20$.Therefore,thefault-currentcompensationeffectof ASC is relatively weak during the transient process, namely, the actual fault current $\dot{I}f$ is relatively high, which can result in high phase-to-ground voltage for the faulty phase. With the development of SLG fault, the oscillation component with $f1$ is damped and disappears, the main frequency of the resonant ground system is f0. The capacitive component of the fault current is suppressed by ASC, resulting in a reduction of the phase-to-ground voltage of the faulty phase. Fig. 2 illustrates the phase relationship between three-phase voltage and ZSV.

The ZSV rises slowly, especially in case of HIFs. If the traditional fault detection method is utilized, the moment when the fault is detected lags behind the actual fault occurrence moment by several cycles. This delay may result in the inaccurate extraction of fault transient features, making it challenging to determine the faulty feeder or faulty section.

2) *SLG fault disappears:* Based on Thevenin's theorem and the circuit superposition principle, the equivalent zero-sequence circuit can be derived, which is shown in Fig. 3. And the fault-disappearance characteristics of ZSV can be analyzed.

Fig. 3 shows an RLC parallel second-order circuit, if SLG fault disappears, it is a zero-input response circuit. The differential equation of the circuit can be obtained.

d2$iL(t)$ Ld$iL(t)$ + LC +$i2L(t)$=0(4)$dt3Rf$d$t$

Its characteristic equation is

$\frac{L}{R}s$ + = LC $s2$ +10 (5)

$iL(t)$= A e$^{s1t}$ + A$_2$e$^{s2t}$ (6)

A = $\frac{u(0)C}{L s s}$
1 = − ( 1$u2$ 0 L s C() s) ( 1 2 (7)
A

$s12$ ± C= f· 2 1 [ ()3Rf √ √ ( 1 ) 3 R 2 LC √ [ √ 2 (8)

where $A1$ and $A2$ are characteristic constants determined by the initial values of the dynamic element, $s1$ and $s2$ are two solutions of characteristic equations. According to Fig. 3, the expression of ZSV can be obtained.

= d$iL(t)u0(t)uC(t)=uL(t)=L$ (9)d$t$

Based on (7) and (9), the expression of ZSV can be rewritten as

$u0t$
=$L$·(A$s1t1s1e$+A$s$)()22$s2et$(10)

Due to the damping, the ZSV gradually attenuates after SLG fault disappears.

Consequently, when a HIF occurs in the resonant ground system, the ZSV rises slowly. When this fault disappears, the ZSV decreases slowly.

### *B. Analysis of ZSV in the Unbalanced Distribution Network*

The problem of unbalanced line parameters is common in distribution networks, which causes a presence of ZSV. In the resonant ground system, the ZSV will be higher, which may lead to the mal-detection of SLG faults. According to Fig. 1 and Kirchhoff's current law, the following expression can be derived

$(\dot{E}$ ) ) $\dot{U}\dot{Y}$ ( (A$\dot{U}$0A $\dot{E}$B$\dot{U}$0$\dot{Y}$B $\dot{E}$C$\dot{U}$0$\dot{Y}$C $\dot{U}$0$YL$0(11) where $\dot{Y}$A , $\dot{Y}$B , $YC$ and $YL$ are the phase-to-ground total admittance and the admittance of ASC, respectively, which can be expressed as

$\dot{Y}$A =jω$C$A +$G$A $\dot{Y}$B =jω$C$B +$G$B
$\dot{Y}$C =jω$C$C +$G$C $\dot{Y}$=1(ω) (12)
$L$sc $L$

Under the condition of unbalanced line parameters, the ZSV can be expressed as

AA $\dot{E}$B$Y$B $\dot{E}$CC= − $\dot{E}$ · $\dot{Y}$ · + · · + · $\dot{Y}$ · $\dot{Y}$
A$Y$BC$L$ · + · +$\dot{Y}$ · +$\dot{Y}$ · $U$0bd (13)
= $\dot{Y}$ · = · +$\dot{Y}$ · +$\dot{Y}$ ·
$j$12Assuming αe0, $Y$A B C,(13)canbe rewritten as · $\dot{Y}$ · +2 · + ·

( )$\dot{E}$AAααC$U$0bd=1(14)$\dot{Y}$B $Y$ + $\dot{Y}$ 2

Consequently, in scenarios where the distribution network exhibits no mismatch and a constant damping ratio, the greater the imbalance of line parameters, the higher the amplitude

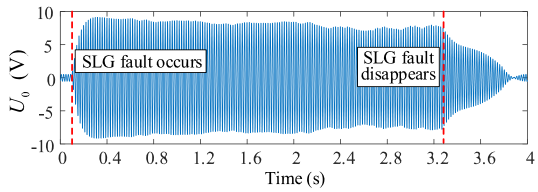


Fig. 4. The waveform of ZSV.

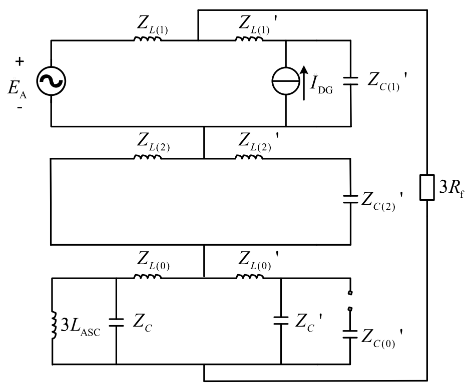


Fig. 5. The three-sequence network of distribution network with IIDGs.

of ZSV. Taking the ZSV waveform of a transient SLG fault in a substation as an example, the SLG fault lasts for about 3s. The characteristics of ZSV during fault occurrence and disappearance are √depictedinFig.4.TheratiooftheZSVtransformeris(103)kV/6.5 V.

According to the requirements of the relay protection systems, reliable fault detection is particularly important. On the other hand, most of the existing faulty feeder and faulty section identification algorithms generally utilize transient features. Therefore, the accurate capture of fault occurrence moment is critical.

### C. Analysis of Zero-Sequence Voltage in Distribution Network With IIDGs

In general, the distribution network feeder is interconnected with the distributed generators (DGs) via a transformer with a Star/Delta winding configuration [13], [30]. Therefore, the zero-sequence component on the DG side will not be injected into the distribution feeder. However, the inverter-interfaced distributed generators (IIDGs) operating in current control mode can be equivalently represented as a positive-sequence current source in parallel with filtering capacitors [31], [32]. Consequently, the three-sequence network of a distribution network with IIDGs operating at power frequency is depicted in Fig. 5. The positive-sequence, negative-sequence, and zero-sequence inductive reactance (including line and transformer inductive reactance) from the fault point to the distribution network side are denoted by $Z$ , , and , espectively‴$L(1)ZL(2)ZL(0)$r.Similarly,$Z$ $L(1)$, $ZL(2)$, $ZL(0)$ denote the inductive reactance from the fault point to IIDGs side, respectively. $\dot{Z}_C$ is the total capacitive impedance from the fault point to the distribution network side. $Z'_C$ is the total capacitive impedance from the fault point to IIDGs side. $Z'$, $'$ and $'$ $C(1)ZC(2)\ ZC(0)$

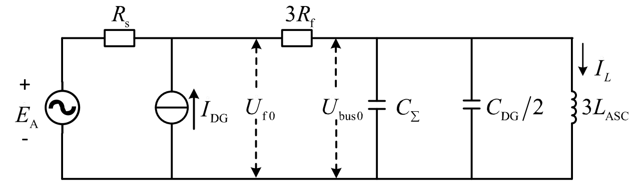


Fig. 6. The simplified three-sequence network.

represent the positive-sequence, negative-sequence, and zero-sequence capacitive impedance of the distributed generators, respectively.

The capacitive impedance of the line significantly exceeds the inductive reactance, allowing the inductive reactance of the line to be neglected. If the source impedance is considered, the simplified three-sequence network is illustrated in Fig. 6.

$\dot{U}_{f0}$ is the fault point voltage, $U$bus0 is ZSV of the bus.

The fault point voltage $Uf0$, affected by the harmonics resulting from IIDGs, can be represented as

$$\dot{U}_{f0} = U_0\sin(\omega_0 t+\phi_0) + U_1\sin(\omega_1 t+\phi_1) + \cdots + U_n\sin(\omega_n t+\phi_n) \quad (15)$$

where $\dot{U}_0\sin(\omega_0 t+\phi_0)$ is the ZSV component of the source voltage of faulty phase. $U_i\sin(\omega_i t+\phi_i)$,($i$ =1,...,$n$)isthe harmonic voltage of IIDGs. $U_i$, $\omega_i$ and $\phi_i$, ($i$ = 1,...,$n$), are the amplitude, angular frequency, and inception angle, respectively. According to Fig. 6 and Kirchhoff's law, $\dot{U}_{f0}$ can be represented as

) ] ∑ ∑CDGd$U$30$U$(f0Ubus)0RC2+(16)2d$t$ $U_{f0}(s) = 0$ $i$

where $C_{DG}$ is the equivalent capacitance of distributed generator. After Laplace transform, $U$bus0 can be expressed as

$n$ $i$ [ 3 $C\Sigma+CL$ DGASC 2+ $\phi$ ) ] $s2i$ $(s)+RC$ (17) $i$ 1 ] ∑ )+$C$3DG3$L\Sigma+CDGf$2ASC$C$2

It can be observed that the harmonic voltage produced by IIDGs overlaps with the fundamental frequency ZSV. The zero-sequence component on the IIDGs side cannot be interconnected with the distribution network side, and only the equivalent positive-sequence current source affects ZSV. In general, the amplitude of the harmonic voltage is lower than the amplitude of the fundamental frequency ZSV. According to equation (17), the SLG fault characteristics of harmonic voltage are consistent with the fundamental frequency ZSV. Furthermore, when the source impedance is negligibly small, it becomes equivalent to a parallel connection of $\dot{E}_A$ and $\dot{I}_{DG}$, the current source representing IIDGs can also be neglected.

Consequently, when an SLG fault occurs, the influence of IIDGs on the amplitude of ZSV is relatively minor and does not change the main characteristics of ZSV variation.

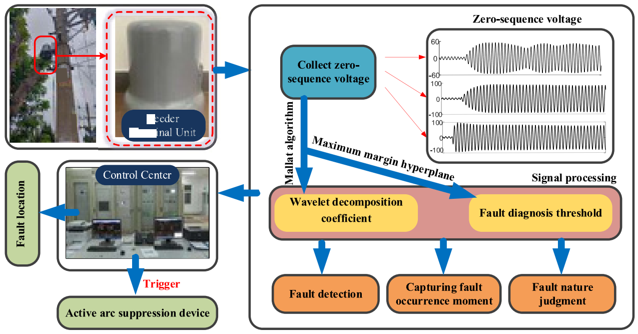


Fig. 7. The diagram of fault diagnosis method.

TABLE I
FILTER COEFFICIENT

| Coefficients | $h_{-1}$ | $h_0$ | $h_1$ | $h_2$ | $g_0$ | $g_1$ |
|---|---|---|---|---|---|---|
| Value | 0.125 | 0.375 | 0.375 | 0.125 | -2.000 | -2.000 |

## III. DIAGNOSIS METHOD OF SLG FAULT

Fig. 7 shows the comprehensive framework of the proposed SLG fault diagnosis method. The proposed algorithm is implemented in the FTU which can collect ZSV in real time. The fault detection, fault occurrence moment capture, and fault nature estimation can be realized by the Mallat algorithm and maximum margin hyperplane. The fault diagnosis results are sent to the control center for further processing of SLG faults. This includes determining the faulty feeder or section by the faulty feeder or faulty section identification algorithms, and triggering the active arc suppression device quickly when the distribution network is equipped with this device.

### A. Signal Multiscale Decomposition

Multi-resolution analysis can effectively retain and analyze the local information of the signal [25]. The Mallat algorithm is applied to the multi-scale decomposition of signals. This method can realize the wavelet decomposition by obtaining the filter coefficients of each scale. The recurrence equation is

$$\begin{cases} S^{(p)}_{2^j} f(n) = \sum_k h_k S^{(2p)}_{2^{j-1}} f(n-2^{j-1}k) & (p \text{ is even}) \\ S^{(p)}_{2^j} f(n) = \sum_k g_k S^{(2p-1)}_{2^{j-1}} f(n-2^{j-1}k) & (p \text{ is odd}) \end{cases} \quad (18)$$

$$W_{2^j} f(n) = \sum_k g_k S_{2^{j-1}} f(n-2^{j-1}k) \quad (19)$$

where $S_{2^j}$ is the approximate component of the scale, $W_{2^j}$ is the detailed component of the $j$th scale, $h_k$ is the low-pass filter coefficient, $g_k$ is the high-pass filter coefficient. The signal decomposition diagram is shown in Fig. 8, where $f_s$ is the sampling frequency.

Because the derivative function of cubic B-spline is symmetrical, the linear phase of response filter can be guaranteed to avoid phase distortion. It is utilized as the mother wavelet function of Mallat signal decomposition algorithm, the coefficients are shown in Table I.

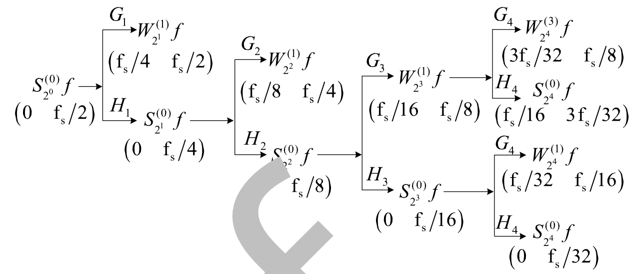


Fig. 8. Signal decomposition process.

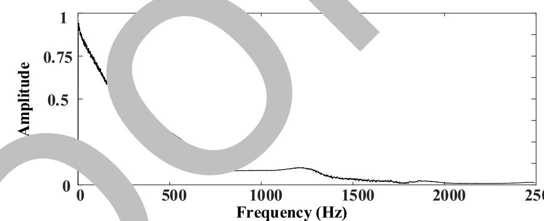


Fig. 9. ZSV envelope spectrum of SLG fault.

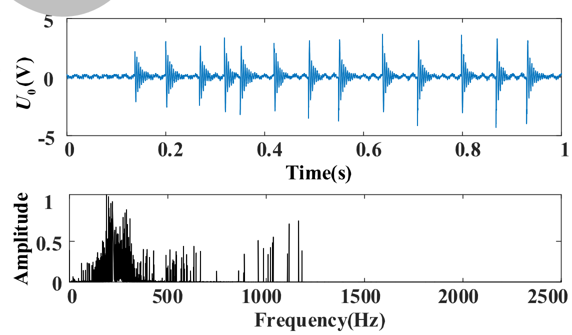


Fig. 10. ZSV of intermittent faults and its marginal spectrum.

To obtain the appropriate number of decomposition levels, the envelope spectrum is used to analyze the frequency composition of ZSV waveform illustrated in Fig. 4. The frequency band components of ZSV are calculated by the envelope spectrum, which is normalized and shown in Fig. 9.

When an SLG fault occurs, the main components of ZSV are concentrated in the low-frequency band, especially within 0-400Hz. In addition, intermittent faults are special cases in SLG faults, where multiple transient faults occur in a short period, so the ZSV in these cases has more high-frequency components [25]. The ZSV of an actual fault obtained from a substation and its normalized marginal spectrum is shown in Fig. 10.

Therefore, the ZSV is decomposed into four layers by Mallat algorithm. The approximate component $S^{(0)}_{2^4} f$ (0-312.5Hz) and the detailed component $W^{(3)}_{2^4} f$ (937.5-1250Hz) are taken as the analysis object of the fault diagnosis.

### B. Thresholds Calculation Method Based on Maximum Margin Hyperplane

Unbalanced line parameters may also cause ZSV to rise as mentioned previously. In general, if an SLG fault occurs, the ZSV will further increase, so the amplitude of the

ZSV between normal and SLG faults can be distinguished. Therefore, the appropriate threshold ε can be obtained by the maximum-margin hyperplane which is defined as $\boldsymbol{w}$T · $\boldsymbol{x}$ + $b$ = 0 [33], [34]. The distance from each input vector to the hyperplane can be expres

$y_i$ ×($\boldsymbol{w}$T·$\boldsymbol{x}_i$+)sedas$b$≥1,∀$i$∈(1,2,...,$N$)(20)

where $y_i$ is the label of input vector, $\boldsymbol{x}_i$ is the input vector, (×) represents performing a product operation, (·) represents performing a dot multiplication operation, $\boldsymbol{w}$ and $b$ are the weight and bias, respectively. The following relationships can be satisfied.

{T·,$y\boldsymbol{w}\boldsymbol{x}i$+$b$=≥1$i$=1

≤

{− (21)1,$y_i$=−1 ∃ $\boldsymbol{w}$T·$\boldsymbol{x}k$1+$b$=1($\boldsymbol{x}k$1,$\boldsymbol{x}k$2),$s.t.$

( $\boldsymbol{w}$T· (22)$\boldsymbol{x}k$2+$b$=−$b$=−$\boldsymbol{w}$T·$\boldsymbol{x}$ T$k$1+$\boldsymbol{w}$·) 1$\boldsymbol{x}k$2/2 (23)

Construct all inputs into a one-dimensional array, the inputs with positive labels are $x1$, $x2$, . . . , $xm$, the inputs with negative labels are $xm$ +1,$xm$+2,...,$xN$, $N = m + n$. Since the input one-dimensional variable, $\boldsymbol{w}$T can be equivalent to $w$, and the following re

{lationshipcanbeobtained.$wxk$1=min($wx$1,...,$wxm$)$wx$

$k$2 = (24)max($wxm$+1,...,$wxm$+$n$)

To calculate the threshold, the expression of the maximum-margin hyperplane can be rewritten as

$w$ε1 +$b$=0 (25)

Based on (21)–(25), the threshold can be calculated.

ε1 =(min($wx$1,...,$wx$)+···max($wx$,...,$w$T$m$ $m$+1 $xN$))/2$w$ (26)

Calculate $w$ by the Lagrange multiplier method [34], the relevant expression is as follows.

1

// // L(w,b,λ)

// // // w2 // ∑N= + λ$i$(1−$y_i$($wx_i$+$b$))2 $i$=1

{$s.t.$λ$i$≥0{(27)∂$L$($w$,$b$,λ)$w$=∑0$w$0∂1λ$xy$∂(,,λ)→

∑−$Ni$=$iii$=$LwbNb$=(28)00∂$i$=1λ$iy_i$=

The ZSV approximate components of unbalanced line parameters$S$(0)$f$ (0)40bdandSLGfault$S$farebroughtinto(2 2 240$f$ 6), the threshold can be calculated

ε γ = (0) (0)1(min($wS$4$f$($f$),...,$wS$4$f$210 2$m$(0$f$))+··· max($wS$(0) $f$ +,...,$wS$(0)4$m$()4$fN$(0bd)2$w$(29)210bd))/2

## C. Capture the Fault Occurrence Moment

For the accurate extraction of fault transient features, it is very important to process the signals at the fault occurrence moment. Therefore, VMD-TEO algorithm is introduced to capture the fault occurrence moment. Where, VMD refers to an adaptive, non-recursive signal processing method [35], which can decompose the input signal $u$ into multiple sub-signals with specific sparsity.

$k$ $k$ { { ∑ )]min{$Kj$−2$j$ω$t$,ω}$k$=1∂$t$∂($t$)+π$tuk$($t$)$e$2(31)

$u$ $u$ = ∑$u$}{⌊$s.tK.k$=

where δ() $t$ istheDiracfunction,$uk$isthedecomposedsignal, ω$k$ is the center frequency of each component. Obtaining the optimal solution of constraint expression by alternating direction multiplier method. TEO can quickly and accurately track the instantaneous changes of signal energy, which is defined as

[]d$st$2 d2[]=()−·$s$($t$)ψ$s$($t$) $s$($t$) (32)dt d$t$2

where $s(t)$ is the original signal. For discrete signals, the forward difference method is used to obtain the discrete expression of TEO.

$$\psi[s(n)] = (s(n))^2 - s(n+1)\times s(n-1) \quad (33)$$

TEO of the first modal component is calculated, the moment when the first spike in the spectrum is located is the fault occurrence moment.

## D. Judgment Method of SLG Fault Disappearance

According to the waveform illustrated in Fig. 4, after the SLG fault disappears, ZSV starts to decrease, and its variation is large, which can be used as a criterion for detecting fault disappearance. However, when the fault resistance varies non-linearly, the ZSV also varies significantly. To distinguish the variation of ZSV is caused by fault disappearance or other disturbances, the approximate component variation and detailed component variation of ZSV are calculated.

The variations of approximate component and detailed component can be calculated by

$S$ ($i$) = $S$(0) 24$f$($i$) − $S$(0) 24$f$($i$ − $L$)

$W$ ($i$) = $W$(3) 24$f$($i$) − $W$(3) 24$f$($i$ − $L$) (34)

where $L$ is the number of sampling points in a cycle.

Analyzing the field waveform of ZSV illustrated in Fig. 4, with the time window of 3s to 3.6s being intercepted. Its approximate component variation and detailed component variation are shown in Fig. 11(a). And Fig. 11(b) depicts the variation of approximate component and detailed component in the disturbance.

It can be seen that the detailed component is more sensitive to waveform change than the approximate component, the difference in approximate component variation between the fault disappearance and disturbance is more obvious. To distinguish

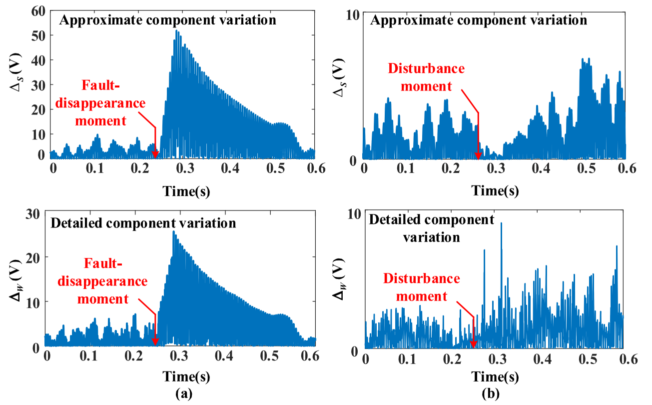


Fig.11. Approximatecomponentvariationanddetailedcomponentvariation of ZSV: (a) SLG fault disappears, (b) SLG fault with disturbance.

TABLE II
CALCULATED FAULT THRESHOLDS

| Network configuration and fault conditions | | | Appropriate threshold (V) |
|---|---|---|---|
| Overcompensation of ASC (%) | Asymmetry of line (%) | Fault resistance(Ω) | |
| 5 | 1 | 1000 | 2590 |
| | | 3000 | [illegible] |
| | | 5000 | [illegible] |
| 5 | 0.5 | 3000 | [illegible] |
| | 1.5 | | [illegible] |
| | 2 | | [illegible] |
| 3 | 1 | 3000 | 1680 |
| 6 | | | 1440 |
| 9 | | | [illegible] |

from disturbance, the proposed maximum margin hyperplane is used to calculate the optimal threshold ε3 for detecting fault disappearance. If the approximate component variation exceeds ε3, it is considered that the SLG fault has disappeared.

In addition, according to Fig. 10, because of the short duration of intermittent faults, if the approximate component falls below the threshold ε1 or the detailed component falls below the threshold ε2, it also indicates that the fault has disappeared.

### E. Online Calculated Method of the SLG Fault Thresholds

According to Section II, the applicable fault threshold varies based on the different distribution network components, such as the asymmetry of line parameters, overcompensation of arc suppression coils, and fault resistance values. Although the optimal threshold can be calculated from the maximum margin hyperplane, the corresponding thresholds differ for distribution networks with different fault conditions. Based on the simulated data, the appropriate fault detection thresholds under different configurations and SLG fault conditions are presented in Table II.

Based on the analysis results of Section II-B, in case of low overcompensation of ASC and high asymmetry of line parameters, the amplitude of ZSV is high during normal operation of the distribution network, possibly exceeding the fault threshold associated with high overcompensation of ASC and low asymmetry of line parameters, leading to misjudgment of SLG faults. Therefore, the SLG fault detection thresholds should be calculated in real time. The comparison coefficient λ can be defined and used to avoid misjudgment caused by this situation:

$$\lambda = \frac{S_2^{(0)} f_{\text{train2}}}{S_2^{(0)} {}_4 f_{\text{train1}}} \quad (35)$$

where $S(0)4f$ 2 train1 is the approximate component under normal conditions in the training samples, $S(0)4f$ 2 train2 is the approximate component under fault conditions in the training samples. The threshold-comparison coefficient ελ between 1 and λ can be calculated by maximum margin hyperplane. Therefore, the fault threshold of approximate component ε1 can be expressed as

$$\varepsilon_1 = \varepsilon_\lambda \cdot \max S_2^{(0)} {}_4 f_{\text{test1}} \quad (36)$$

where $\max S(0)(4f$ 2 test1) is the approximate-component maximum value of ZSV collected in real time under normal condition. Similarly, ε2 can also be calculated. Additionally, ε3 is directly calculated based on the approximate component variation of ZSV through the maximum margin hyperplane.

### F. SLG Fault Diagnosis Process

The proposed fault diagnosis method can rapidly detect SLG faults, capture the fault occurrence moment, and estimate the fault nature. The flowchart for a fault diagnosis cycle is shown in Fig. 12. According to the IEEE standard 1234-2019 [36], the time criterion for the fault nature estimation is set to 10s. Consequently, the time for a fault diagnosis cycle is 10s. The specific steps are as follows.

Step 1: Collect ZSV signal in real time and calculate its approximate component $S(0)f$ 24 and detailed component $W(3)$ 24f.

Step 2: According to Section III-E, the fault-disappearance threshold ε3 can be calculated. And the SLG fault detection thresholds ε1 and ε2 are calculated in real time based on the sampled ZSV.

Step 3: An SLG fault occurs when the approximate or detailed component of ZSV exceeds the fault detection threshold ε1 or ε2. Meanwhile, the real-time calculation of these thresholds is stopped and the current thresholds are stored. And the fault occurrence moment is captured by the VMD-TEO algorithm.

Step 4: In the fault diagnosis cycle, if the fault does not satisfy the fault disappearance criterion, then the SLG fault is determined as the prolonged fault.

Step 5: The main characteristic of intermittent faults is that they occur several times in a short period and the duration is very short [37]. The transient faults exhibit longer fault durations than intermittent faults. Nevertheless, the transient faults disappear after a certain duration and are not characterized by recurrence. Therefore, in a fault diagnosis cycle, a fault is transient if it satisfies the fault disappearance criterion and does not recur. If it recurs more than three times, the fault is intermittent.

Step 6: The transient features are extracted based on the captured fault occurrence moment, which can be utilized to identify faulty feeder and faulty section.

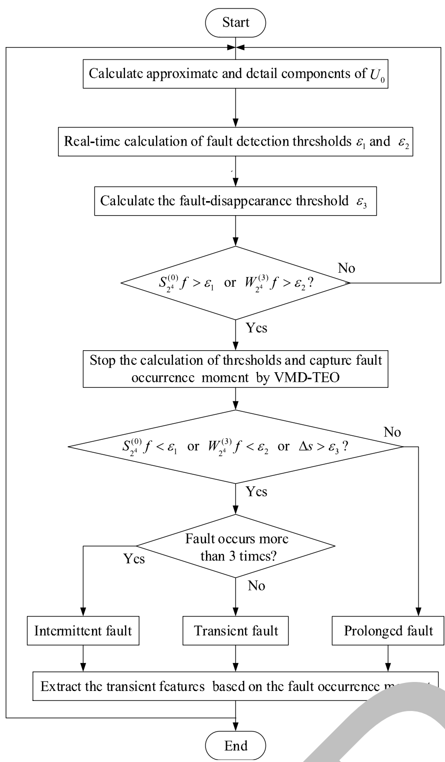


Fig. 12. SLG fault diagnosis flow chart.

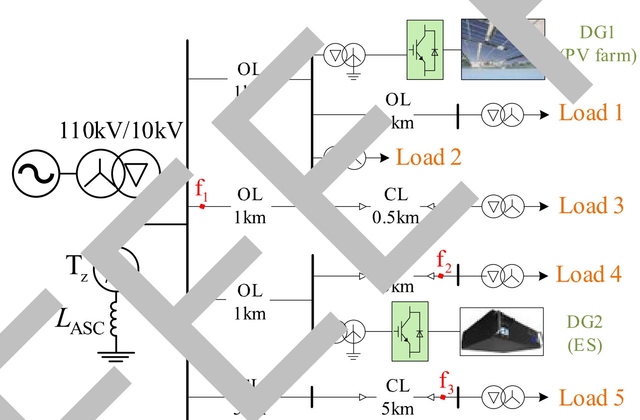


Fig.13. Simulationmodelof10kVactivedistributionnetwork,thepower supplies of DG1 and DG2 are 0.15MW and 0.1MW, respectively.

Step 7: After completing one cycle of fault diagnosis, the next cycle of diagnosis is started, realizing the online detection of SLG faults.

## IV. SIMULATIONVERIFICATION

The effectiveness of the proposed fault diagnosis method is verified by the 10kV active distribution network simulation model, which is shown in Fig. 13. Where $Tz$ is the grounding transformer, $f1$, $f2$, $f3$ are the fault points, OL is the overhead line, and CL is the cable line. Meanwhile, the IIDGs, such as photovoltaic (PV) farms and energy storage (ES) systems, are connected in the distribution network, which serves to verify the correctness of the analysis results in Section II-C.

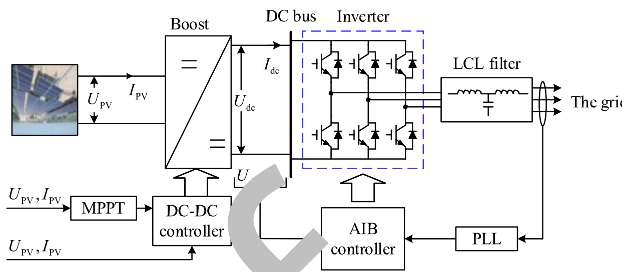


Fig. 14. The control block diagram of the PV system.

TABLE III
LINE DISTRIBUTION PARAMETER

| Line type | $r_0/r_1$(Ω/km) | $c_0/c_1$($\mu$F/km) | $l_0/l_1$(mH/km) |
|---|---|---|---|
| OL | 0.2750/0.1250 | 0.0054/0.0096 | 4.6000/1.3000 |
| CL | [illegible] | 0.2800/0.3390 | 1.0190/0.2550 |

The control block diagram of the PV system is illustrated in Fig. 14. In the process of DC/DC control and inverter control, the adaptive integral backstepping (AIB) control scheme has high robustness [38]. Therefore, this non-linear controller is employed for the PV system.

Meanwhile, the ES system is connected to the grid through DC/AC converter, and can equivalently operate as an IIDG when it is in a power supply state [39], [40]. A basic two-level (2L) converter is employed as the converter within ES system, and its control strategy is droop control, which includes phase-locked loop (PLL) control, outer loop control, and inner loop control. The control block diagram of the 2L converter within the ES system is similar to that of the inverter utilized in the PV system [39].

The distribution lines adopt the pi-type equivalent model, the line distribution parameters are listed in Table III.

### A. SLG Fault Detection

*1) Calculate the SLG fault threshold:* In the distribution network, the asymmetry of OL parameters is typically within 1.5% and the asymmetry of CL parameters is typically within 0.5% [41]. The model shown in Fig. 13 has been simulated with the ASC overcompensation of 2-10% with a step of 2%, and the fault resistances of 10 , 50 , 500 , and 5000 . From the simulation, 30 sets of data representing normal operating conditions and their corresponding 120 sets of data representing SLG fault conditions can be obtained. The relative threshold ελ can be calculated as 2.7 by the maximum margin hyperplane.

The Mallat algorithm can quickly decompose the original signal, which only requires 46 sample points of discrete data, this process takes only 4.6ms with a sample rate of 10kHz. Therefore, the fault thresholds can be calculated quickly.

However, if the line parameters and the loads are symmetrical, the ZSV under normal conditions is relatively low, which can lead to the fault thresholds being small, thus resulting in the fault detection algorithm being too sensitive. Therefore, a reference value of approximate component $S(0)$ 24 $fref$ is set to improve the robustness of fault detection algorithms. The

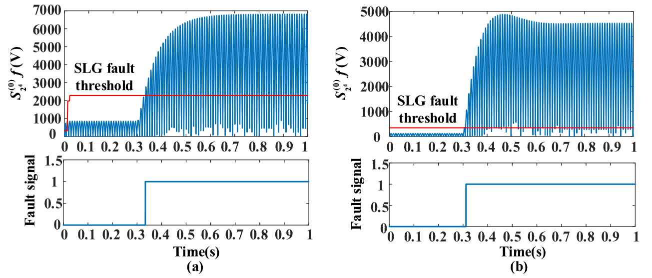


Fig.15. The detection results of SLG fault: (a) Approximate component exceeds $S^{(0)}_{2\text{ref}}$ $4f$ under normal conditions, (b) Approximate component does not exceed $S^{(0)}_{2\text{ref}}$ $4f$ under normal conditions.

TABLE IV
THE ANALYSIS RESULTS OF FAULT DETECTION

| Line type | Overcompensa-tion of ASC | Asymmetry | Fault resistance (Ω) | Number of cases | Correct rate |
|---|---|---|---|---|---|
| OL | 2% - 10% | 0.5% - 1.5% | 10, 50, 500,5000 | 25 | 100% |
| CL | 2% - 10% | 0.2% - 0.5% | | 30 | 100% |

following relationship should be satisfied.

$$\varepsilon_1 = \begin{cases} \lambda_\varepsilon \cdot (\max S_{24}^{(0)} f_1), & \max(S_2^{(0)} f_1) \geq S_{24}^{(0)} f_{ref} \\ \lambda_\varepsilon \cdot S_{24}^{(0)} f_{ref}, & \max(S_2^{(0)} f_1) < S_{24}^{(0)} f_{ref} \end{cases} \quad (37)$$

Consider the ZSV of a normally operating neutral ungrounded system under the condition of maximum line parameter imbalance, $S(0)f_{24\,ref}$ can be calculated as 120V.

2) *Analysis of simulation results of SLG faults:* Because the Mallat algorithm simplifies the signal decomposition process, thresholds under normal system conditions can be quickly calculated. Take the cases where approximate components exceed $S(0)f_{24\,ref}$ and those do not exceed $S(0)f_{24\,ref}$ under normal conditions as examples, the fault detection results are illustrated in Fig. 15.

The rate of correct SLG fault detection under different situations is shown in Table IV.

3) *Influence of non-fault disturbances:* The non-fault disturbances discussed in this paper include load switching (LS), capacitor switching (CS), and DG off-grid (DGO) [42]. In Fig. 16, $t_d$ is the occurrence moment of disturbance, the detection results of these three non-fault disturbances are demonstrated. It can be observed that the approximate components of non-fault disturbances do not exceed the SLG fault threshold. For LS and CS, the change in ZSV is due to a surge in the transient switch. Meanwhile, because the line parameters are asymmetrical, after the switching action, the ZSV will oscillate. Because the amplitude of this oscillation is attenuated, the ZSV does not exceed the threshold which is calculated in real time. In addition, because the primary sides of DG transformers are delta connected and not grounded [13], when the DGs are disconnected, the ZSV does not change significantly.

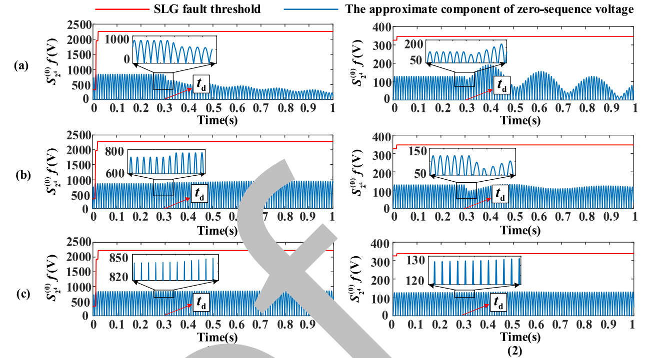


Fig.16. The detection results of non-fault disturbances: (a) CS, (b) LS, (c) DGO, and (1) Approximate component exceeds $S(0)_{24\,fref}$ under normal conditions, (2) Approximate component does not exceed $S(0)_{24\,fref}$ under normal conditions.

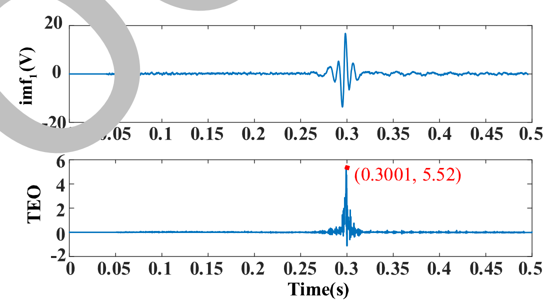


Fig. 17. The waveforms of the first modal component and its TEO.

*B. Capture the Occurrence Moment of SLG Fault*

In resonant ground systems, there is a time interval between the fault detected moment and the actual fault occurrence moment. The higher the fault resistance, the longer this time interval will be. Part of the difficulty in detecting HIFs is due to inaccurate estimation of fault occurrence moment. In this paper, the VMD-TEO algorithm is utilized to capture the SLG fault occurrence moment. The simulation data collected from the distribution network depicted in Fig. 13 is utilized as the example, a time window with a length of 0.5s is chosen, assuming the SLG fault occurs at 0.3s and the fault resistance is 2000 . Meanwhile, the Gaussian white noise is added to ZSV with a signal-to-noise ratio of 5dB. After the 5-layer decomposition of ZSV by utilizing VMD, the waveforms of the first modal component (imf1) and its TEO are shown in Fig. 17.

It can be observed that the estimation error of detected fault occurrence moment is only 0.1ms. Taking into account the potential for extreme fault scenarios in actual distribution networks, noise above 2000Hz is filtered out during the data processing stage to enhance the robustness of the proposed fault diagnosis method.

*C. SLG Fault Nature Estimate*

According to the requirements of the relay protection system, the accurate estimation of SLG fault nature is important. The simulation obtained 150 sets of ZSV data with transient, intermittent and permanent fault, which include

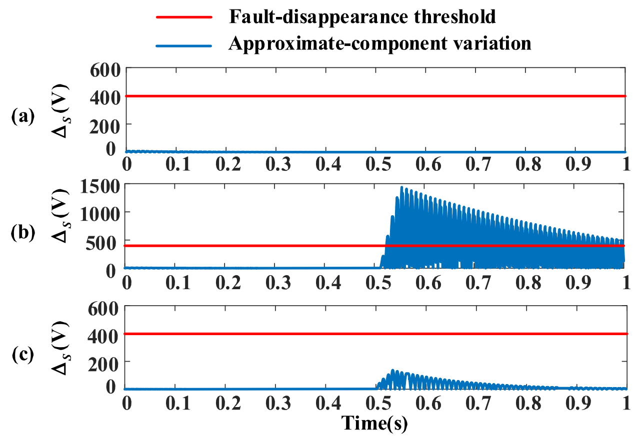


Fig.18. SLGfaultdisappearancejudgment:(a)Prolongedfault,(b)Transient fault, (c) Fault resistance variation.

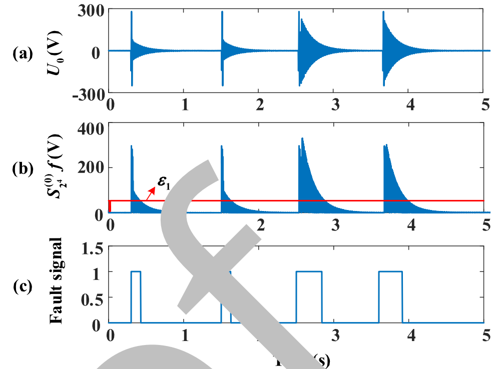


Fig.19. Intermittentfaultdetectionanalysis:(a)ZSV,(b)Theapproximate component, (c) The fault signal.

TABLEV
FAU LTOCCURRENCE ANALYSIS RESULTS

| Inception angle(°) | Fault resistance(Ω) | $\eta_1$ | $\eta_2$ | $t_1$ (s) | $t_2$ (s) |
|---|---|---|---|---|---|
| ≤ 45 | ≤ 2000 | 100% | 100% | [illegible] | [illegible]0002 |
| | >2000 | 100% | 100% | [illegible]79 | [illegible]03 |
| >45 | ≤ 2000 | 100% | 100% | 0.019 | [illegible] |
| | >2000 | 100% | 100% | 0.023 | [illegible] |

"$\eta_1$" means the rate of correct fault detection, "$\eta_2$" [illegible]ns the r[illegible] of correct fault disappearance detection, "$t_1$" means the maximum [illegible]val between the fault detected moment and the actual fault occurrence mo[illegible]. "$t_2$" means the maximum error of fault occurr[illegible] moment.

TABLE VI
THERESULTS OF SENSITIVITY ANALYSIS

| Fault position | $\eta_1$ | $\eta_2$ | $t_2$ (s) |
|---|---|---|---|
| $f_1$ | 100% | 100% | 0.002 |
| [illegible] | 100% | 100% | 0.006 |

### D. Sensitivity Analyses of the Proposed Method

The impedance of the line leads to a certain voltage, which can usually be ignored. It is defined as the distribution line voltage in this paper. Without considering the distribution line voltage, the ZSV measured at different positions is consistent. However, when the line is very long, the influence of the distribution line voltage on ZSV at different measurement different fault resistances, different line parameters asymmetry, positions along this line cannot be ignored. and different arc suppression coil overcompensation degrees. Furthermore, when the HIF occurs, the small amplitude Then, the threshold for fault disappearance is calculated as of ZSV and the long transient process are challenging for 398V by the maximum margin hyperplane. The distinguished SLG fault diagnosis. Therefore, it is necessary to analyze the results between prolonged faults and transient faults are shown applicability of the proposed fault diagnosis method in these inFig.18. cases.

Only when the SLG fault disappears, the approximate- According to Fig. 13, it is assumed that the SLG fault component variation of ZSV will exceed the fault occursatthebeginningofashortline$f$1 ortheendofa disappearance threshold. Through the active distribution long line f3, with fault resistances of 10k , 13k , 16k , network model illustrated in Fig. 13, the cases of different and fault inception angles of 0∘, 30∘, 60∘, 90∘, respectively. fault resistances and different line asymmetry are simulated, The overcompensation of ASC is 5% and 10%, respectively. and the fault diagnosis results are shown in Table V. It can And the asymmetry degree of the line parameters is 1%. be observed that the proposed fault diagnosis method can Consequently, there are 24 sets of fault samples for both $f$1 accurately detect the occurrence and disappearance of SLG and f3. Assuming a perfect instrument transformer is used, faults, and accurately capture the fault occurrence moment. measurement errors can be disregarded, the test results are According to the analysis of intermittent faults, if an SLG shown in Table VI. fault occurs and disappears more than three times within 10s, It can be observed that the proposed fault diagnosis method it can be judged as intermittent fault. Under the condition of still can reliably detect the occurrence and disappearance of intermittent faults, if the approximate component falls below SLG faults. However, when the fault occurs at the end of the the threshold ε1 or the detailed component falls below the long line and the fault resistance is high, the estimation results threshold ε2, it indicates that the fault has disappeared. Take of the fault occurrence moment have a relatively large error. the approximate component as an illustrative example. The That is because the ZSV amplitude of a HIF is relatively low. It characteristics of the intermittent faults and the detection result is difficult to accurately detect the small changes in the ZSV if andareshowninFig.19. themeasurementpositionisfarfromthefaultpoint.InFig.20, It can be observed from Fig. 19(c) that the proposed method a violin plot is utilized to illustrate the estimation error of fault effectively detects the occurrence and disappearance of SLG occurrence moment, which includes 288 sets of simulation faults, which ensures the reliable identification of intermittent data. The median estimation error of fault occurrence moment SLGfaults. is0.1ms.Themaximumpositiveerrorandminimumnegative

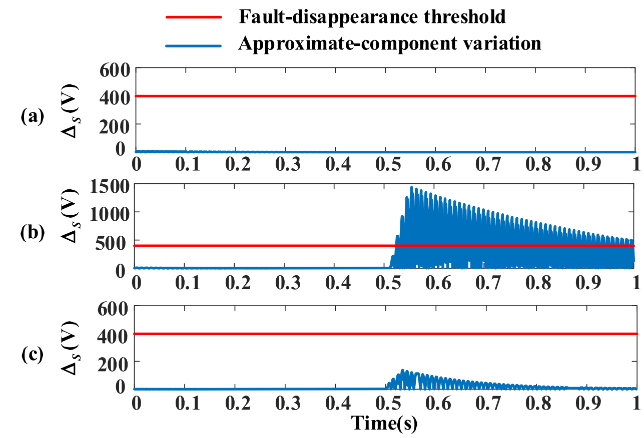


Fig. 20. The error of fault occurrence moment for the proposed method.

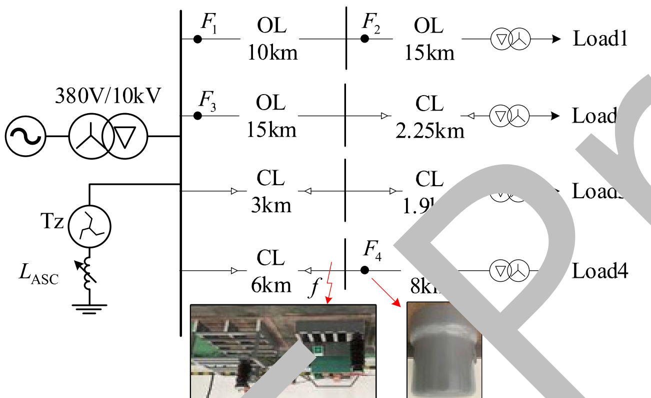


Fig. 21. Power distribution network experimental structure.

TABLE VII
SIMULATED LINE PARAMETERS

| Line number | Line type | Capacitive current(A) | Simulated length(km) | Total capacitance($\mu$F) |
|---|---|---|---|---|
| 1 | OL | 3.4 | 25 | 10.8 |
| 2 | OL&CL | 8 | 17.35 | |
| 3 | CL | 10 | 4.9 | |
| 4 | CL | 20 | 9.7 | |

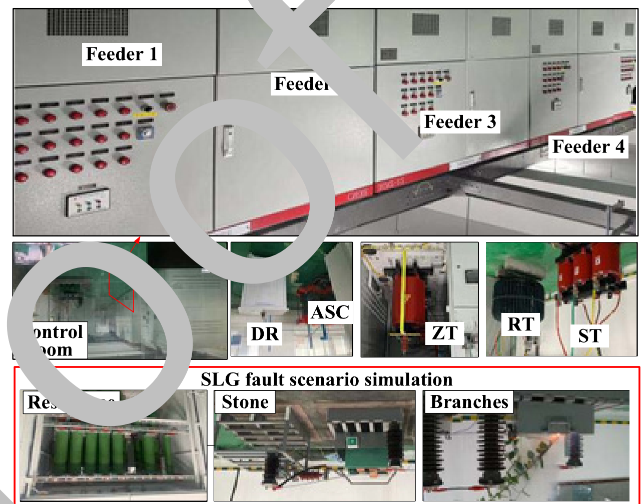


Fig. 22. 10kV experimental platform and the simulated SLG fault scenarios.

error are 6ms and -3.6ms, respectively. It can be observed that the proposed method provides a relatively accurate estimation of fault occurrence moment.

In addition, to mitigate the influence of long distribution lines on the precision of fault occurrence moment estimation, the algorithms introduced in this paper are integrated within FTUs of overhead lines. Consequently, several measurement points are configured in the distribution network so that the fault position and the measurement position are as close as possible.

## V. Experimental and Field Validation

### A. Experimental Platform and Data Analysis

The effectiveness of the proposed fault diagnosis method is further verified by the 10kV distribution network prototype experimental platform. The structure of this experimental system is shown in Fig. 21, where *Fi*, *i* =1,2,...,4,indicates the installation position of the FTUs. The line parameters are shown in Table VII.

Through this experimental platform, the conditions of resistance grounding fault, stone grounding fault and branches grounding fault are simulated. Among them, the fault resistances of resistance grounding faults are 100 , 200 , 2000 , 5000 , 10k , and 16k , respectively, including the simulation of HIFs. The 10kV prototype experimental platform is shown in Fig. 22, which includes four feeders and simulated fault scenarios. These feeders are simulated through Pi RL components. In Fig. 22, ZT is the grounding transformer, DR is the damping resistance, RT is the regulator transformer, and ST is the step-up transformer. The designed FTU and its connection method are shown in Fig. 23. The fault diagnosis algorithm is embedded in the Raspberry Pi of the designed FTU. The ZSV is collected and stored by the AD7606 chip and STM32F407 microcontroller and then sent to the Raspberry Pi which has two processes running the fault detection algorithm and the fault occurrence moment capture algorithm respectively. When the microcontroller has stored a 0.5s length of ZSV, it is sent to the Raspberry Pi and starts the next 0.5s acquisition. In addition, the SLG fault detection algorithm calculates the fault threshold in real time and it takes only 0.038s to judge whether the fault occurs. If an SLG fault occurs, it stops the threshold calculation and saves the current thresholds, and then sends the ZSV data for the first 0.2s and the last 0.1s of that detection point to the fault occurrence moment capture algorithm. It takes only 0.12s to calculate the fault occurrence moment. Therefore, the real-time diagnosis of SLG faults can be realized.

The branches grounding faults are usually accompanied by fault arcing and have the characteristics of HIFs. The burning of branches and changes in arc length usually result in unstable fault resistance. Therefore, to better illustrate the effectiveness of the proposed fault diagnosis method, take the branches grounding fault as an example. The detection results of SLG fault occurrence and disappearance are shown in Fig. 24. When the fault signal is 1, it indicates that an SLG fault has occurred. When the fault signal is 0, it indicates

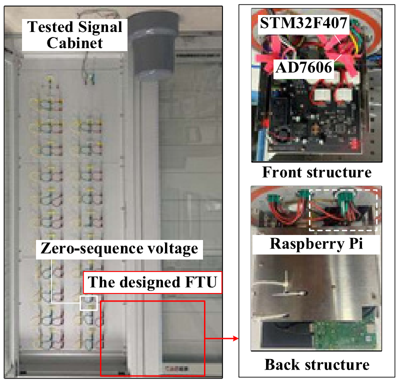


Fig. 23. The designed FTU and the exhibition of its connection method.

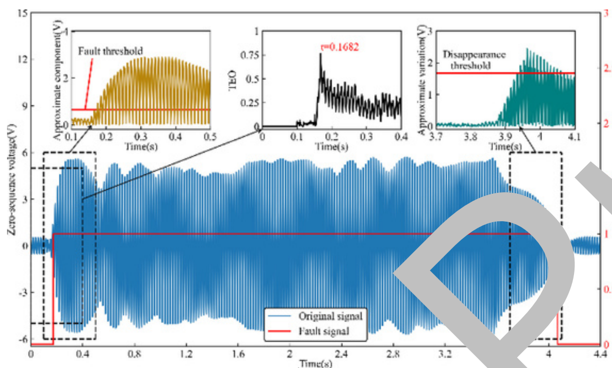


Fig. 24. Experimental data analysis.

TABLE VIII
EXPERIMENTAL DATA ANALYSIS RESULTS

| Fault scenarios | Number of cases | $\eta_1$ | $\eta_2$ | $t_2$ (s) |
|---|---|---|---|---|
| Resistance grounding | 54 | 100% | 100% | 0.0030 |
| Stone grounding | 21 | 100% | 100% | 0.0005 |
| Branches grounding | 24 | 100% | 100% | 0.0012 |

"$t_2$" means the maximum error to capture the moment of fault.

that the fault disappears. Furthermore, the proposed fault diagnosis method can capture the fault occurrence moment. Table VIII shows the detection results of different fault scenarios.

Several non-fault disturbances are simulated on the experimental platform to verify the robustness of the proposed method, including transformer energization, cold load pickup, hot load removal, and rotating load connection. Among them, the cold load pickup is simulated by connecting the load of Feeder 2, which is initially in a non-operational state, during the normal operation of the experimental system. And the hot load removal is simulated by subsequently removing the load of Feeder 2 after the experimental system has operated with this load for 15 hours. Taking the approximate component of ZSV as an example, the detection results of these non-fault disturbances are shown in Fig. 25. It can be observed that these non-fault disturbances will not be misclassified as SLG faults.

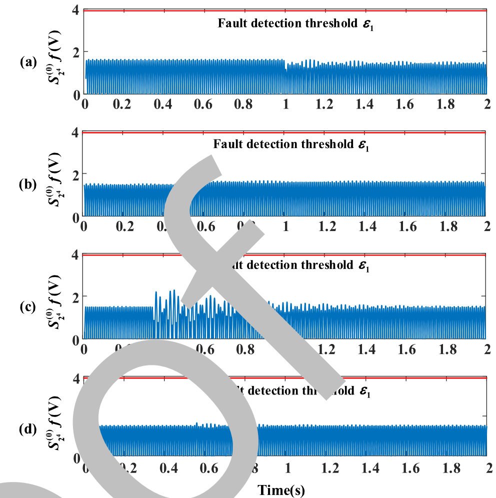


Fig.25. The approximate component of ZSV: (a) Transformer energization, (b) Cold load pickup, (c) Hot load removal, (d) Rotating load connection.

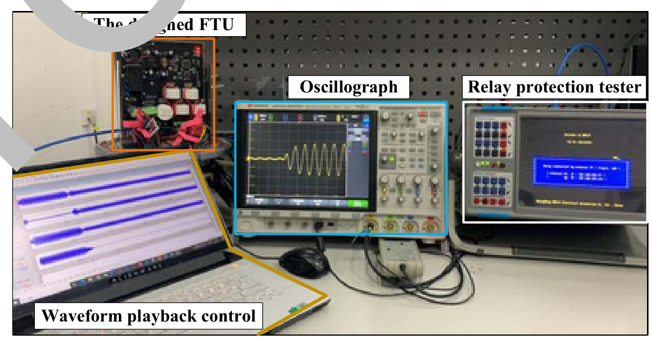


Fig. 26. The field data playback.

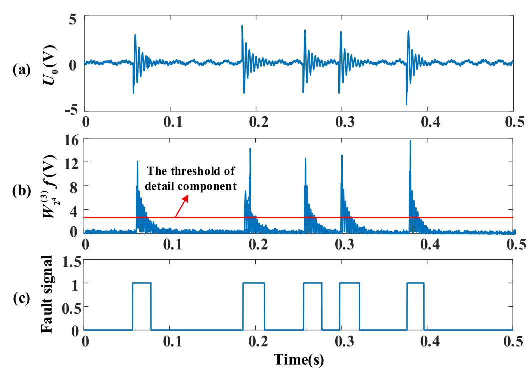


Fig.27. Intermittent fault detection analysis: (a) Original signal, (b) The detailed component of ZSV, (c) Fault signal.

### B. Field Data Analysis

Through the relay protection tester, the fault record data in the actual distribution network can be reproduced. The waveform testing for the actual distribution network is depicted in Fig. 26. Taking the fault data of a master station as an example, the test results of the fault occurrence and disappearance are illustrated in Fig. 27. It can be observed that the SLG fault repeatedly occurs 5 times in a short period. Therefore, it is the data of intermittent fault. Table IX shows the analysis results of

TABLE IX
FIELD DATA ANALYSIS RESULTS

| Fault type | Number of cases | $\eta_1$ | $\eta_2$ | $\eta_3$ | $t_2$ (s) |
|---|---|---|---|---|---|
| Intermittent fault | 5 | 100% | 100% | 100% | 0 |
| Transient fault | 19 | 100% | 94.74% | 94.74% | 0.0010 |
| Prolonged fault | 15 | 93.33% | 100% | 93.33% | 0.0002 |

" $\eta_3$ " means the rate of correct fault nature estimation.

TABLE X
RESULTS OF THE COMPARISON

| Method | $\eta_1$ | $\eta_4$ | $t_2$(s) |
|---|---|---|---|
| TFD | 72.46% | 82% | 0.038 |
| EWT-DFE | 94.92% | 94% | 0.029 |
| MM | 79.71% | 56% | 0.010 |
| DWT | 91.30% | 60% | 0.008 |
| The proposed method | 99.27% | 98% | 0.002 |

the field data which is measured from an operating distribution system.

It can be observed that the feasibility and effectiveness of the proposed fault diagnosis method have been verified.

### C. Comparison and Analysis

The effectiveness of different methods for SLG fault diagnosis is compared by the experimental data and field data. The criterion for traditional fault detection methods (TFD) is whether the ZSV exceeds 15% of the phase voltage [11]. In [13], a fault detection method based on empirical wavelet transform and differential faulty energy (EWT-DFE) is proposed. In [17], mathematical morphology (MM)-based method is utilized to detect SLG faults. And a discrete wavelet transform (DWT)-based fault detection method is proposed in [25]. Through the experimental data and field data, fault detection correct rate η1, non-fault disturbance detection correct rate η4, and maximum error for fault occurrence moment *t2* of these methods and the proposed method are calculated and listed in Table X. There are 138 sets of SLG fault data, and 50 sets of non-fault disturbance data, including CS, LS and transformer energization, etc.

It can be observed that the proposed fault diagnosis method exhibits the highest correct rate in fault detection as well as non-fault disturbance detection. Although EWT-DFE-based method also achieves high correct rate, it does not provide an estimation of the fault occurrence moment. Consequently, the error of fault occurrence moment is relatively large. In a resonant ground system, if the faulty feeder and section identification algorithms have not been triggered within one cycle after the occurrence of an SLG fault, the feature difference between the healthy and faulty feeders may decrease. Therefore, the minor error in fault occurrence moment can contribute to enhancing the rate of correct faulty feeder and faulty section identification.

In addition, the fault diagnosis thresholds of the proposed method are calculated in real time through the maximum margin hyperplane and can be better adapted to different asymmetric conditions of the distribution network. Meanwhile, the proposed method also integrates three functions, namely fault detection, fault occurrence moment capture and fault nature estimation, improving the utilization rate of the designed device.

## VI. CONCLUSION

This paper has proposed an SLG fault diagnosis method for resonant ground systems. Firstly, the ZSV is collected by FTU. Then, the approximate and detailed components are calculated and compared separately with their thresholds which are the optimal thresholds calculated by the maximum margin hyperplane in real time. Finally, effective fault detection and accurate fault nature estimation have been realized. The following key conclusions can be obtained from this research work:

1) The proposed fault diagnosis method calculates the SLG fault thresholds in real time, which makes the method highly robust to line parameter imbalance and non-fault disturbances. Its feasibility and applicability are verified by simulation, experimental and field data.

2) The proposed fault diagnosis method has the capability of accurately capturing the moment of fault occurrence, which has been verified. It is of great importance in accurately extracting the transient features of SLG faults and improving the accuracy of faulty feeder and faulty section identification.

3) This method integrates the three functions of fault detection, fault occurrence moment capture and fault nature estimation with the same requirements for hardware devices and measurement signals, which improves the applicability and equipment utilization of the designed FTU.

## REFERENCES

[1] "IEEE PES distribution system analysis subcommittee." Distribution Test Feeders. 2017. [Online]. Available: http://ewh.ieee.org/soc/ pes /dsacomtestfeeders/index.html
[2] H. L. Willis, "Power delivery systems," in *Power Distribution Planning Reference Book*, 2nd ed. Boca Raton, FL, USA: CRC Press, 2004, pp. 29–35, ch. 1.
[3] Y.Duetal.,"Singleline-to-groundfaultedlinedetectionofdistribution systems with resonant grounding based on feature fusion framework," *IEEE Trans. Power Del.*, vol. 34, no. 4, pp. 1766–1775, Aug. 2019.
[4] M.A.Barik,A.Gargoom,M.A.Mahmud,M.E.Haque,H.Al-Khalidi, and A. M. Than Oo, "A decentralized fault detection technique for detecting single phase to ground faults in power distribution systems with resonant grounding," *IEEE Trans. Power Del.*, vol. 33, no. 5, pp. 2462–2473, Oct. 2018.
[5] J. Li, Y. Liu, C. Li, D. Zeng, H. Li, and G. Wang, "An FTU-based method for locating single-phase high-impedance faults using transient zero-sequence admittance in resonant grounding systems," *IEEE Trans. Power Del.*, vol. 37, no. 2, pp. 913–922, Apr. 2022.
[6] C.Ozansoy,"Performanceanalysisofskewnessmethodsforasymmetry detection in high impedance faults," *IEEE Trans. Power Syst.*, vol. 35, no. 6, pp. 4952–4955, Nov. 2020.
[7] S.-R. Nam, S.-H. Kang, S.-J. Ahn, and J.-H. Choi, "Single line-to-ground fault location based on unsynchronized phasors in automated ungrounded distribution systems," *Electr. Power Syst. Res.*, vol. 86, pp. 151–157, May 2012.
[8] D. R. R. Penido, L. R. De Araujo, V. T. S. Rodrigues, and K. B. Do Nascimento, "An analytical zero sequence method to locate fault in distribution systems rich in DG," *IEEE Trans. Smart Grid*, vol. 13, no. 3, pp. 1849–1859, May 2022.
[9] Y. Zhang, S. Xie, and S. Shu, "Decentralized optimization of multi-area interconnected traffic-power systems with wind power uncertainty," *IEEE Trans. Ind. Info.*, vol. 19, no. 1, pp. 133–143, Jan. 2023, doi: 10.1109/TII.2022.31528-15.

[10] *Microgrid Protection Systems*, IEEE Power Energy Soc., Piscataway, NJ, USA, Jul. 2019.

[11] X.Wangetal.,"Locationofsinglephasetogroundfaultsindistribution networks based on synchronous transients energy analysis," *IEEE Trans. Smart Grid*, vol. 11, no. 1, pp. 774–785, Jan. 2020.

[12] A. N. Milioudis, G. T. Andreou, and D. P. Labridis, "Enhanced protection scheme for smart grids using power line communications techniques—Part-II: Location of high impedance fault position," *IEEE Trans. Smart Grid*, vol. 3, no. 4, pp. 1631–1640, Dec. 2012.

AQ2 [13] J. Gao, X. Wang, X. Wang, A. Yang, H. Yuan, and X. Wei, "A high-impedance fault detection method for distribution systems based on empirical wavelet transform and differential faulty energy," *IEEE Trans. Smart Grid*, vol. 13, no. 2, pp. 900–912, Mar. 2022.

[14] Z. Y. Zheng, M. F. Guo, N. C. Yang, and T. Jin, "Single-phase flexible arc suppression device based on BSC-SOGI-PLL method for distribution networks," *Int. J. Electr. Power Energy Syst.*, vol. 121, Oct. 2020, Art. no. 106100.

[15] M. F. Guo, X. D. Zeng, D. Y. Chen, and N. C. Yang, "Deep-learning-based earth fault detection using continuous wavelet transform and convolutional neural network in resonant grounding distribution systems," *IEEE Sensors J.*, vol.18, no.3, pp.1291–1300, Feb. 2018.

[16] K. Sarwagya, S. De, and P. K. Nayak, "High-impedance fault detection in electrical power distribution systems using moving sum approach," *IET Sci. Meas. Technol.*, vol. 12, no. 1, pp. 1–8, Jan. 2018.

[17] S. Gautam and S. M. Brahma, "Detection of high impedance fault in power distribution systems using mathematical morphology," *IEEE Trans. Power Syst.*, vol. 28, no. 2, pp. 1226–1234, May 2013.

[18] A. N. Milioudis, G. T. Andreou, and D. P. Labridis, "Detection and location of high impedance faults in multiconductor overhead distribution lines using power line communication devices," *IEEE Trans. Smart Grid*, vol. 6, no. 2, pp. 894–902, Mar. 2015.

[19] E.M.Limaetal.,"Highimpedancefaultdetectionmethodbasedonthe short-time Fourier transform," *IET Gener., Transmiss. Distrib.*, vol. 12, no. 11, pp. 2577–2584. Apr. 2018.

[20] D. Li, A. Ukil, K. Satpathi, and Y. M. Yeap, "Hilbert–Huang transform based transient analysis in voltage source converter interfaced direct current system," *IEEE Trans. Ind. Electr.*, vol. 68, no. 11, pp. 11014–11025, Nov. 2021.

[21] M. F. Guo, N. C. Yang, and L. X. You, "Wavelet-transform based early detection method for short-circuit faults in power distribution networks," *Int. J. Elect. Power Energy Syst.*, vol. 99, pp. 706–721, Jul. 2018.

[22] X. Chen, "Real wavelet transform-based phase information extraction method: Theory and demonstrations," *IEEE Trans. Ind. Electr.*, vol. 56, no. 3, pp. 891–899, Mar. 2009.

[23] X. Wang et al., "High impedance fault detection method based on variational mode decomposition and Teager–Kaiser energy operators for distribution network," *IEEE Trans. Smart Grid*, vol. 10, no. 6, pp. 6041–6054, Nov. 2019.

[24] D. A. Gadanayak and R. K. Mallick, "Interharmonics based high impedance fault detection in distribution systems using maximum overlap wavelet packet transform and a modified empirical mode decomposition," *Int. J. Elect. Power Energy Syst.*, vol. 112, pp. 282–293, Nov. 2019.

[25] C. Lin, W. Gao, and M. F. Guo, "Discrete wavelet transform-based triggering method for single-phase earth fault in power distribution systems," *IEEE Trans. Power Del.*, vol. 34, no. 5, pp. 2058–2068, Oct. 2019.

[26] Y. Liang, K.-J. Li, Z. Ma, and W.-J. Lee, "Multilabel classification model for type recognition of single-phase-to-ground fault based on KNN-Bayesian method," *IEEE Trans. Ind. Appl.*, vol. 57, no. 2, pp. 1294–1302, Mar./Apr. 2021.

[27] X. Liang, S. A. Wallace, and D. Nguyen, "Rule-based data-driven analytics for wide-area fault detection using synchrophasor data," *IEEE Trans. Ind. Appl.*, vol. 53, no. 3, pp. 1789–1798, May 2017.

[28] Q. Cui and Y. Weng, "Enhance high impedance fault detection and location accuracy via μ-PMUs," *IEEE Trans. Smart Grid*, vol. 11, no. 1, pp. 797–809, Jan. 2020.

[29] J. Fang, Y. Yan, H. Zhang, H. Wang, and Y. Wang, "Research on fault section location method of distribution networks with arc suppression coil grounding based on energy leakage function," *IET Gener. Transm. Distrib.*,vol. 14, no.25, pp. 6097–6106, Dec. 2020.

[30] J. Yuan, Y. Hu, Y. Liang, and Z. Jiao, "Faulty feeder detection for single line-to-ground fault in distribution networks with DGs based on correlation analysis and harmonics energy," *IEEE Trans. Power Del.*, vol. 38, no. 2, pp. 1020–1029, Apr. 2023.

[31] Z. Shuai, C. Shen, X. Yin, X. Liu, and Z. J. Shen, "Fault analysis of inverter-interfaced distributed generators with different control schemes," *IEEE Trans. Power Del.*, vol. 33, no. 3, pp. 1223–1235, Jun. 2018.

[32] W.-M. Guo, L.-H. Mu, and X. Zhang, "Fault models of inverter-interfaced distributed generators within a low-voltage microgrid," *IEEE Trans. Power Del.*, vol. 32, no. 1, pp. 453–461, Feb. 2017.

[33] R. Jiang and Y. Zheng, "Series arc fault detection using regular signals and time-series reconstruction," *IEEE Trans. Ind. Electr.*, vol. 70, no. 2, pp. 2026–2036, Feb. 2023.

[34] J. C. Burges, "A tutorial on support vector machine for pattern recognition, *Data Min. Knowl. Discovery*, vol. 2, no. 2, pp. 121–167, Jun. 1998.

[35] L. Xie, L. Luo, Y. Li, Y. Zhang, and Y. Cao, "A traveling wave-based fault location method employing VMD-TEO for distribution network," *IEEE Trans. Power Del.*, vol. 35, no. 4, pp. 1987–1998, Aug. 2020.

[36] *IEEE Guide for Fault Locating Techniques on Shielded Power Cable Systems*, IEEE Standard 1234-2019, Jun. 12, 2019.

[37] M. M. Alamuti, H. Nouri, R. M. Ciric, and V. Terzija, "Intermittent fault location in distribution feeders," *IEEE Trans. Power Del.*, vol. 27, no. 1, pp. 96–103, Jan. 2012.

[38] M. M. Rahman, S. P. Biswas, M. R. Islam, M. A. Rahman, and K. M. Muttaqi, "An advanced nonlinear controller for the LCL-type three-phase grid-connected solar photovoltaic system with a DC–DC converter," *IEEE Syst. J.*, vol. 16, no. 2, pp. 3203–3214, Jun. 2022.

[39] G. Wang et al., "A review of power electronics for grid connection of utility-scale battery energy storage systems," *IEEE Trans. Sustain. Energy*, vol. 7, no. 4, pp. 1778–1790, Oct. 2016.

[40] G. G. Farivar et al., "Grid-connected energy storage systems: State-of-the-art and emerging technologies," *Proc. IEEE*, vol. 111, no. 4, pp. 397–420, Apr. 2023.

[41] W. Wang, X. Gao, B. Fan, X. Zeng, and G. Yao, "Faulty phase detection method under single-line-to-ground fault considering distributed parameters asymmetry and line impedance in distribution networks," *IEEE Trans. Power Del.*, vol. 37, no. 3, pp. 1513–1522, Jun. 2022.

[42] W.H.Kwon,G.W.Lee,Y.M.Park,M.C.Yoon,andM.H.Yoo,"High impedance fault detection utilizing incremental variance of normalized even order harmonic power," *IEEE Trans. Power Del.*, vol. 6, no. 2, pp. 557–564, Apr. 1991.


**Jiahao Lin** (Student member, IEEE) was born in Fujian, China, in 1997. He received the B.S. degree in electric machines and electric apparatus from Fuzhou University, Fujian, in 2019, where he is currently pursuing the Ph.D. degree. His main research interest is the detection and location of single-line-to-ground fault in distribution network.

**Moufa Guo** (Member, IEEE) was born in Fujian, China, in 1973. He received the B.S. and M.S. degrees in electrical engineering from Fuzhou University, Fuzhou, China, in 1996 and 1999, respectively, and the Ph.D. degree in electrical engineering from Yuan Ze University, Taoyuan, Taiwan, in 2018.

Since 2000, he has been with Fuzhou University, where he is currently a Professor with the College of Electrical Engineering and Automation. His research interests include the information processing, protection control, and flexible arc suppression of single-line-to-ground fault in distribution networks.

**Qiteng Hong** (Senior Member, IEEE) received the B.Eng. (Hons.) and Ph.D. degrees in electronic and electrical engineering from the University of Strathclyde, Glasgow, U.K., in 2011 and 2015, respectively, where he is currently a Senior Lecturer (Associate Professor). His main research interest is on power system protection and control in future networks with high penetration of renewables. He is a member of IEEE Working Group P2004 and IEEE Task force on Cloud-Based Control and Co-Simulation of Multi-Party Resources in Energy Internet, and he also was a Regular Member of the completed CIGRE WG B5.50.

**Run Jiang** (Student Member, IEEE) received the B.S. and M.S. degrees from Fuzhou University, Fujian, China, in 2016 and 2020, respectively. He is currently pursuing the Ph.D. degrees in electrical engineering with Fuzhou University and Yuan Ze University, Taoyuan, Taiwan. His main research interests include measurement technology on fiber-optic current sensing, arc model, and AC/DC series arc fault detection.

AUTHOR QUERIES

AUTHOR PLEASE ANSWER ALL QUERIES

**PLEASE NOTE: We cannot accept new source files as corrections for your paper. If possible, please annotate the PDF proof we have sent you with your corrections and upload it via the Author Gateway. Alternatively, you may send us your corrections in list format. You may also upload revised graphics via the Author Gateway.**

**Carefully check the page proofs (and coordinate with all authors); additional changes or updates WILL NOT be accepted after the article is published online/print in its final form. Please check author names and affiliations, funding, as well as the overall article for any errors prior to sending in your author proof corrections. Your article has been peer reviewed, accepted as final, and sent in to IEEE. No text changes have been made to the main part of the article as dictated by the editorial level of service for your publication.**

AQ1: Please confirm or add details for any funding or financial support for the research of this article.

AQ2: References [13] and [16] were the same in your originally submitted manuscript, so Reference [16] has been deleted and the remaining references (and their in text citations) have been renumbered. Please check and confirm that they are correct as set.

# An Earth Fault Diagnosis Method Based on Online Dynamically Calculated Thresholds for Resonant Ground Systems

Jiahao Lin, *Student Member, IEEE*, Moufa Guo, *Member, IEEE*, Qiteng Hong, *Senior Member, IEEE*, and Run Jiang, *Student Member, IEEE*



***Abstract*—The primary problem of distribution system protection is single-line-to-ground (SLG) fault, particularly in networks with distributed generators (DGs), where asymmetrical phase sequence components caused by SLG faults may lead to system instability. Currently, the location and suppression methods of SLG faults are based on reliable fault diagnosis. Therefore, considering the imbalance of line parameters, this paper analyzes the component fault characteristics of zero-sequence voltage (ZSV), and proposes a threshold-online-calculating-based SLG fault diagnosis method, which includes fault detection, fault occurrence moment capture and fault nature estimation. Firstly, the ZSV is measured in real time by the designed feeder terminal unit (FTU), which is embedded with the proposed SLG fault diagnosis method. Secondly, the ZSV signal is decomposed by the Mallat algorithm, and the fault diagnosis thresholds are calculated through the maximum margin hyperplane, which is used for fault detection and fault nature estimation. Finally, the fault occurrence moment is captured by variational mode decomposition (VMD) and its Teager Energy Operator (TEO). The proposed SLG fault diagnosis method has been tested in simulation and physical experiments in a 10kV system, the effectiveness and feasibility have been validated.**

***Index Terms*—Distribution network, single-line-to-ground fault, fault diagnosis method, fault occurrence moment capture, fault nature estimation.**

## I. INTRODUCTION

THENEUTRALpointofmedium-voltage(MV)powerfaultdetectioncriteriainthecaseofHIFs.Furthermore,thedistributionsystemsaretypicallyearthedviaanarcamplitudeofZSVrisesslowlyinresonantgroundsystems, suppression coil (ASC) in Europe, Africa, Asia and some parts of North America [1], [2], which is called resonant ground system. The SLG faults account for more than 80% of distribution network line faults, and the ASC is utilized to suppress the fault current [3], [4]. However, during SLG faults, ASC will change the fault characteristics, challenging fault detection and fault location, especially for high impedance faults (HIF) [5], [6]. Furthermore, if the ground fault is accompanied by intermittent arcing, it will lead to arc overvoltage, which could risk the insulation of the line being damaged. In addition, ASC cannot fully suppress the active component and high-frequency harmonics component, which may cause accidents such as fire and large-scale power outages [7].

In addition, smart power distribution systems are gradually being implemented driven by the widespread integration of distributed generators (DGs), and the development of sensing and communication technologies [8]. The smart power distribution systems can realize multi-energy flow synergy, namely "electricity-gas-heat". By combining existing sensing and communication technologies, the information interaction of "source-network-load" can be realized. It helps to improve the self-diagnosis capability which is a pivotal characteristic of the smart power distribution system [9], [10]. When an SLG fault occurs, determining the faulty feeder or faulty section is necessary [11],[12]. Additionally, in a resonant ground system with an active arc suppression device, rapid initiation of the arc suppression device after SLG faults is important [13], [14]. The traditional method mainly uses a ZSV threshold (typically set at 15% of the phase voltage) as thefaultdetectioncriterion[11],[15].Inaneutralungrounded system, the amplitude of ZSV may not satisfy traditional which satisfies the fault detection criterion only after several cycles from the fault occurrence moment. Most of the existing methods extract fault transient features based on the moment when the fault is detected, which may lead to inaccurate transient feature extraction and affect the accuracy of faulty feeder and faulty section identification. Consequently, the rapid detection of SLG faults and accurate capture of fault occurrence moment are crucial.

In recent years, numerous methods for SLG fault detection have been proposed, such as those based on signal processing technology and artificial intelligence (AI). Among them, the

AQ1 Manuscript received 23 March 2023; revised 3 September 2023 and 2 November 2023; accepted 16 December 2023. This work was supported in part by the National Natural Science Foundation of China under Grant 51677030. Paper no. TSG-00419-2023.
Jiahao Lin, Moufa Guo, and Run Jiang are with the College of Electrical Engineering and Automation and the Fujian Key Laboratory of New Energy Generation and Power Conversion, Fuzhou University, Fuzhou 350108, China (e-mail: jh_fd5678@163.com; gmf@fzu.edu.cn; 210110002@fzu.edu.cn).
Qiteng Hong is with the Department of Electronic and Electrical Engineering, University of Strathclyde, G1 1XW Glasgow, U.K. (e-mail: q.hong@strath.ac.uk).
Color versions of one or more figures in this article are available at https://doi.org/10.1109/TSG.2023.3346453.
Digital Object Identifier 10.1109/TSG.2023.3346453

1949-3053

*(Corresponding author: Moufa Guo.)*

Reference [16] detects HIFs by summing the periodic variation ofZSV.Themethodishighlyfeasible,butthedetectiontime is long. In [17], mathematical morphology is utilized as the detection method for HIFs. This method is sensitive to the variation of ZSV but is susceptible to non-fault disturbances. Reference [18] introduces the SLG fault detection method that calculates the input impedance and locates the fault position by the impulse injection in power line communication, but it is suitable only for HIFs.

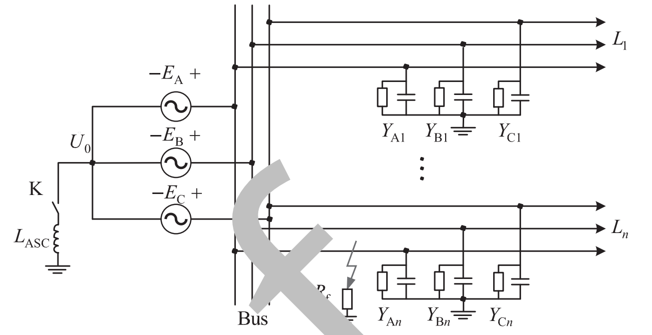


The time-frequency analysis methods retain the time-frequency characteristics of the waveform. This method is widely used because it can extract more transient character- Fig. 1. SLG fault of resonant ground system. istics of SLG faults. The time-frequency analysis algorithm mainly consists of short-time Fourier Transform (STFT) [19], Hilbert-Huang transform (HHT) [20], wavelet transform algorithm. Finally, the criteria for fault nature estimation are (WT) [21], [22], variational mode decomposition (VMD) [23], defined. The effectiveness and feasibility of the proposed SLG empirical mode decomposition (EMD) [24], etc. In [21] faultdiagnosismethodareverifiedbysimulation,experimental and [25], Guo et al. utilized the Mallat algorithm to simplify and field data. wavelet transform and realized the rapid detection of SLG The remainder of the paper is organized as follows. faults. However, the determination of the threshold coefficient Section II analyzes the SLG fault characteristics of ZSV relies on empirical knowledge. The applicability is limited under different conditions. In Section III, the fault diagnosis with high sensitivity to non-fault disturbances, which have method is proposed, including fault detection, fault occurrence a high risk to cause mal-detection of faults. In [13], a HIF moment capture and fault nature estimation. In Section IV, the detection method based on empirical wavelet transform (EWT) proposed method is verified by simulation data. In Section V, is proposed, which realizes the adaptive selection of fault theproposedmethodisverifiedbyexperimentalandfielddata. characteristic frequency bands. However, the methods based Section VI draws the conclusions. on modal decomposition are computationally time-consuming, resultinginalongtimeforfaultdetection. II.ANALYSISOFZERO-SEQUENCEVOLTAGE AI-basedmethodsfindextensiveapplicationinfaultdiag- CHARACTERISTICS nosis and location because of their powerful data processing

*A. The ZSV Analysis of SLG Fault*

capabilities [26], [27], [28]. Unlike traditional methods, AI-basedmethodsdonotrequirespecificthresholdstobedefined. 1)*SLGfaultoccurs:*Fig.1illustratesasimplifiedresonant After the AI algorithms are trained by sample data, they can ground system, assuming that the SLG fault occurs on phase automatically calculate the classification boundary. However, A of *Ln*. AI-based fault detection methods typically require a substan- The ZSV can be represented as tialvolumeofhistoricaldataforlearningandtraining,which

$$\dot U_0 = \dot U_A - \dot E_A \quad (1)$$

presents a significant challenge, as the actual fault data are often limited and difficult to collect. Without sufficient realistic where $\dot U$ is the phase-to-ground voltage of the faulty phase, iningdata,itwillle $\dot E_A$ traadtooverfittingandweakgeneralization*A*isthesourcevoltageofthefaultyphase. abilityofAI-basedmethods. DuringanSLGfault,thefaultcurrentflowstothebus In actual distribution network, the relay protection systems through the fault point. In resonant ground systems, the fault are required to isolate permanent faults quickly. Therefore, current can be expressed as the rapid detection of SLG faults and the estimation of

$$\dot I_f \approx -\dot U_0 \left( j\omega C + G - \frac{1}{j\omega L_{ASC}} \right) \quad (2)$$

thefaultnatureareimportant.However,theexistingfault detectionmethodsmostlyfocusontheidentificationofHIF, ignoring some key issues, such as the speed of fault detection, where $C$ is the total earth capacitance of resonant ground the accurate estimation of fault nature and the impact of system, $G$ is the total earth conductance, and $L_{ASC}$ is the unbalancedlineparameters. inductanceofASC.Ingeneral,topreventtheoccurrenceof Therefore, this paper proposes an SLG fault diagnosis resonance overvoltage, the detuning degree of pre-tuned ASC method based on online dynamically calculated thresholds, istypicallyestablishedat5%[29].Underthenormalfrequency which is capable of detecting faults rapidly, capturing the f0, it can be approximately considered that the inductive occurrence moment of SLG faults and estimating the fault reactance of ASC is equal to the capacitive impedance of total nature. Firstly, when SLG faults occur or disappear under the earth capacitance. With the frequency increasing, the earth condition of unbalanced line parameters, the characteristics of capacitive impedance decreases, and the inductive reactance of ZSV are analyzed. Then, the appropriate thresholds of SLG ASC increases. At the early stage of SLG fault, the dominant fault occurrence and disappearance can be calculated in real frequency of the system (f1) is typically several times f0, thus time by the maximum margin hyperplane. At the same time, the system is seen as capacitive [11]. During the transient the fault occurrence moment can be captured by VMD-TEO process, the relationship between the inductive reactance of

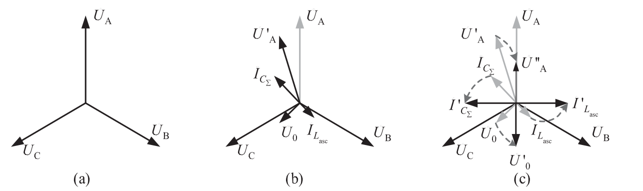


Fig.2. Therelationshipbetweenthree-phasevoltageandZSV:(a)Under normal conditions, (b) SLG fault transient process, (c) SLG fault steady state process.

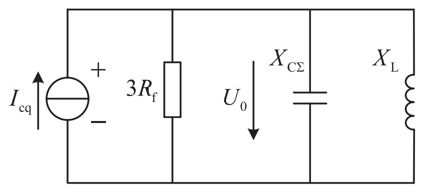


Fig. 3. The equivalent zero-sequence circuit.

ASC and the capacitive impedance of total earth capacitance can be expressed as

()121ωLL≈=CC ω1 0 ω 0ASC ω1 ω0ω0 Σ ω 1 ω1 Σ (ω)

1 ω C Σ = f21 f01 . ω 0 (3)

It can be seen that the ratio between inductance from the ASC and the phase-to-ground capacitance from the network is(f1/f)20.Therefore,thefault-currentcompensationeffectof ASC is relatively weak during the transient process, namely, the actual fault current $\dot{I}f$ is relatively high, which can result in high phase-to-ground voltage for the faulty phase. With the development of SLG fault, the oscillation component with $f1$ is damped and disappears, the main frequency of the resonant ground system is f0. The capacitive component of the fault current is suppressed by ASC, resulting in a reduction of the phase-to-ground voltage of the faulty phase. Fig. 2 illustrates the phase relationship between three-phase voltage and ZSV.

The ZSV rises slowly, especially in case of HIFs. If the traditional fault detection method is utilized, the moment when the fault is detected lags behind the actual fault occurrence moment by several cycles. This delay may result in the inaccurate extraction of fault transient features, making it challenging to determine the faulty feeder or faulty section.

2) *SLG fault disappears:* Based on Thevenin's theorem and the circuit superposition principle, the equivalent zero-sequence circuit can be derived, which is shown in Fig. 3. And the fault-disappearance characteristics of ZSV can be analyzed.

Fig. 3 shows an RLC parallel second-order circuit, if SLG fault disappears, it is a zero-input response circuit. The differential equation of the circuit can be obtained.

d2iL(t) LdiL(t) + LC +i2L(t)=0(4)dt3Rfdt

Its characteristic equation is

LC s2 + L/R s + 1 = 0 (5)

iL(t) = A1 es1t + A2es2t (6)

A1 = u0(0)C / L(s1 − s2)

A2 = − u0(0)C / L(s1 − s2) (7)

s1,2 = − 1 / (2·3Rf·C) ± √[ (1 / (3Rf·C))² − 4/(LC) ] / 2 (8)

where $A1$ and $A2$ are characteristic constants determined by the initial values of the dynamic element, $s1$ and $s2$ are two solutions of characteristic equations. According to Fig. 3, the expression of ZSV can be obtained.

= diL(t)u0(t)uC (t)=uL(t)=L (9)dt

Based on (7) and (9), the expression of ZSV can be rewritten as

u0t

=L·(As1t1s1e+As)()22s2et(10)

Due to the damping, the ZSV gradually attenuates after SLG fault disappears.

Consequently, when a HIF occurs in the resonant ground system, the ZSV rises slowly. When this fault disappears, the ZSV decreases slowly.

*B. Analysis of ZSV in the Unbalanced Distribution Network*

The problem of unbalanced line parameters is common in distribution networks, which causes a presence of ZSV. In the resonant ground system, the ZSV will be higher, which may lead to the mal-detection of SLG faults. According to Fig. 1 and Kirchhoff's current law, the following expression can be derived

(Ė·) ) )U̇Y·( (A0A ĖBU̇0Y·B ĖCU̇0Y·C U̇0YL0(11) where Y·A , Y·B , YC and YL are the phase-to-ground total admittance and the admittance of ASC, respectively, which can be expressed as

Y·A =jωCA +GA Y·B =jωCB +GB

Y·C =jωCC +GC Y·=1(ωLasc) (12)

Under the condition of unbalanced line parameters, the ZSV can be expressed as

AA ĖBYB ĖCC = −Ė · Ẏ · + · · + · Ẏ · Ẏ

AYBCL = Ẏ · = · + Ẏ · + Ẏ · U0bd (13)

Assuming αe0j12, YA B C,(13)canbe rewritten as

( )ĖAAααCU0bd (14) Ẏ · + 2 · + · YB Y

Consequently, in scenarios where the distribution network exhibits no mismatch and a constant damping ratio, the greater the imbalance of line parameters, the higher the amplitude

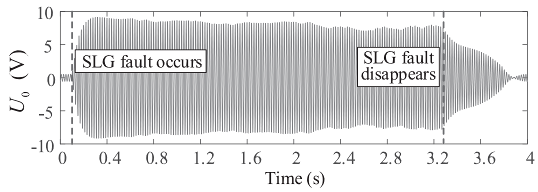


Fig. 4. The waveform of ZSV.

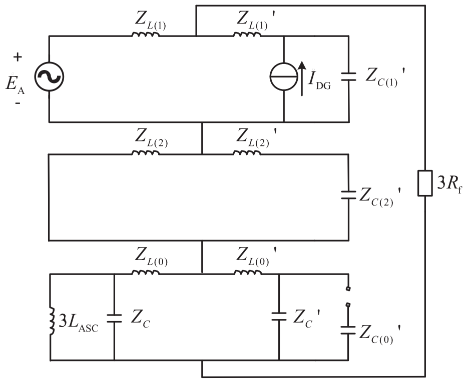


Fig. 5. The three-sequence network of distribution network with IIDGs.

of ZSV. Taking the ZSV waveform of a transient SLG fault in a substation as an example, the SLG fault lasts for about 3s. The characteristics of ZSV during fault occurrence and disappearance are √depictedinFig.4.TheratiooftheZSVtransformeris(103)kV/6.5 V.

According to the requirements of the relay protection systems, reliable fault detection is particularly important. On the other hand, most of the existing faulty feeder and faulty section identification algorithms generally utilize transient features. Therefore, the accurate capture of fault occurrence moment is critical.

### *C. Analysis of Zero-Sequence Voltage in Distribution Network With IIDGs*

In general, the distribution network feeder is interconnected with the distributed generators (DGs) via a transformer with a Star/Delta winding configuration [13], [30]. Therefore, the zero-sequence component on the DG side will not be injected into the distribution feeder. However, the inverter-interfaced distributed generators (IIDGs) operating in current control mode can be equivalently represented as a positive-sequence current source in parallel with filtering capacitors [31], [32]. Consequently, the three-sequence network of a distribution network with IIDGs operating at power frequency is depicted in Fig. 5. The positive-sequence, negative-sequence, and zero-sequence inductive reactance (including line and transformer inductive reactance) from the fault point to the distribution network side are denoted by $Z$ , , and , espectively‴$L(1)ZL(2)ZL(0)$r.Similarly,$Z$ $L(1)$, $ZL(2)$, $ZL(0)$ denote the inductive reactance from the fault point to IIDGs side, respectively. $\dot Z_C$ is the total capacitive impedance from the fault point to the distribution network side. $Z'_C$ is the total capacitive impedance from the fault point to IIDGs side. $Z'$, $'$ and $'$ $C(1)ZC(2)\ ZC(0)$

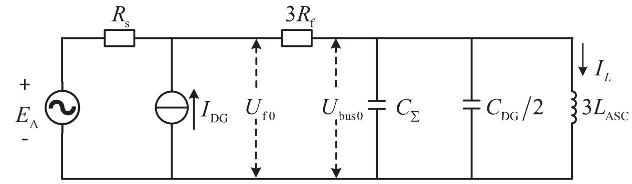


Fig. 6. The simplified three-sequence network.

represent the positive-sequence, negative-sequence, and zero-sequence capacitive impedance of the distributed generators, respectively.

The capacitive impedance of the line significantly exceeds the inductive reactance, allowing the inductive reactance of the line to be neglected. If the source impedance is considered, the simplified three-sequence network is illustrated in Fig. 6.

$\dot U_{f0}$ is the fault point voltage, $U_{bus0}$ is ZSV of the bus.

The fault point voltage $U_{f0}$, affected by the harmonics resulting from IIDGs, can be represented as

$$\dot U_{f0} = U_0\sin(\omega_0 t+\phi_0) + U_1\sin(\omega_1 t+\phi_1) + \cdots + U_n\sin(\omega_n t+\phi_n) \quad (15)$$

where $\dot U_0\sin(\omega_0 t+\phi_0)$ is the ZSV component of the source voltage of faulty phase. $U_i\sin(\omega_i t+\phi_i)$, $(i=1,\ldots,n)$ is the harmonic voltage of IIDGs. $U_i$, $\omega_i$ and $\phi_i$, $(i = 1,\ldots,n)$, are the amplitude, angular frequency, and inception angle, respectively. According to Fig. 6 and Kirchhoff's law, $\dot U_{f0}$ can be represented as

) ] · ∑ =

∑CDGdU30U(0Ubus)0R2C+i2i(16)2dt $U_{bus0}(s)$ $i=0$ [$s\sin\phi_i+\omega_i\cos\phi_i$]

where $C_{DG}$ is the equivalent capacitance of distributed generator. After Laplace transform, $U_{bus0}$ can be expressed as

n i [ 3 C∑+CL DGASC 2+ ϕ ) ) ] s2i (s)+RC i ( 1 ] Σ )+C3DG3L∑+CDGf2ASCC2 (17)

It can be observed that the harmonic voltage produced by IIDGs overlaps with the fundamental frequency ZSV. The zero-sequence component on the IIDGs side cannot be interconnected with the distribution network side, and only the equivalent positive-sequence current source affects ZSV. In general, the amplitude of the harmonic voltage is lower than the amplitude of the fundamental frequency ZSV. According to equation (17), the SLG fault characteristics of harmonic voltage are consistent with the fundamental frequency ZSV. Furthermore, when the source impedance is negligibly small, it becomes equivalent to a parallel connection of $\dot E_A$ and $\dot I_{DG}$, the current source representing IIDGs can also be neglected.

Consequently, when an SLG fault occurs, the influence of IIDGs on the amplitude of ZSV is relatively minor and does not change the main characteristics of ZSV variation.

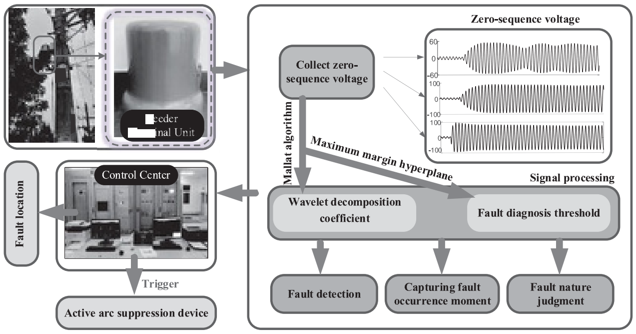


Fig. 7. The diagram of fault diagnosis method.

TABLE I
FILTER COEFFICIENT

| Coefficients | $h_{-1}$ | $h_0$ | $h_1$ | $h_2$ | $g_0$ | $g_1$ |
|---|---|---|---|---|---|---|
| Value | 0.125 | 0.375 | 0.375 | 0.125 | -2.000 | -2.000 |

## III. DIAGNOSIS METHOD OF SLG FAULT

Fig. 7 shows the comprehensive framework of the proposed SLG fault diagnosis method. The proposed algorithm is implemented in the FTU which can collect ZSV in real time. The fault detection, fault occurrence moment capture, and fault nature estimation can be realized by the Mallat algorithm and maximum margin hyperplane. The fault diagnosis results are sent to the control center for further processing of SLG faults. This includes determining the faulty feeder or section by the faulty feeder or faulty section identification algorithms, and triggering the active arc suppression device quickly when the distribution network is equipped with this device.

### A. Signal Multiscale Decomposition

Multi-resolution analysis can effectively retain and analyze the local information of the signal [25]. The Mallat algorithm is applied to the multi-scale decomposition of signals. This method can realize the wavelet decomposition by obtaining the filter coefficients of each scale. The recurrence equation is

$$\begin{cases} S_{2^j}^{(p)} f(n) = \sum_k h_k S_{2^{j-1}}^{(p/2)} f(n - 2^{j-1}k) & (p \text{ is even}) \\ S_{2^j}^{(p)} f(n) = \sum_k g_k W_{2^{j-1}}^{((p-1)/2)} f(n - 2^{j-1}k) & (p \text{ is odd}) \end{cases} \quad (18)$$

$$W_{2^j}^{(p)} f(n) = \sum_k g_k S_{2^{j-1}}^{(p)} f(n - 2^{j-1}k) \quad (19)$$

where $S$ is the approximate component of the $j$th scale, $W_{2^j}$ is the detailed component of the $j$th scale, $h_k$ is the low-pass filter coefficient, $g_k$ is the high-pass filter coefficient. The signal decomposition diagram is shown in Fig. 8, where $f_s$ is the sampling frequency.

Because the derivative function of cubic B-spline is symmetrical, the linear phase of response filter can be guaranteed to avoid phase distortion. It is utilized as the mother wavelet function of Mallat signal decomposition algorithm, the coefficients are shown in Table I.

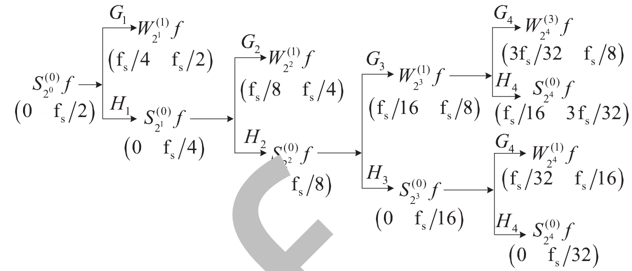


Fig. 8. Signal decomposition process.

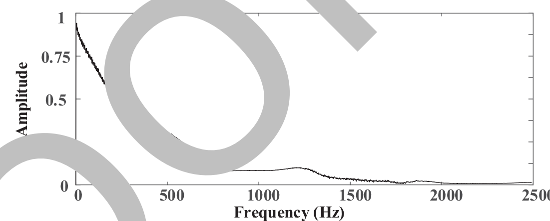


Fig. 9. ZSV envelope spectrum of SLG fault.

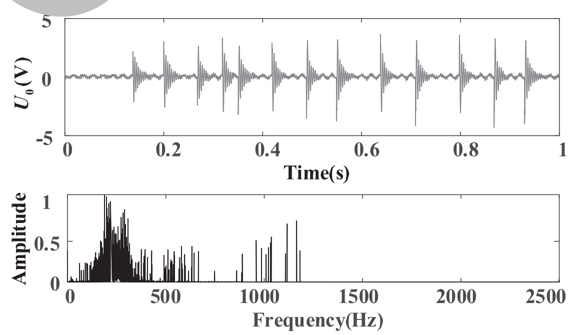


Fig. 10. ZSV of intermittent faults and its marginal spectrum.

To obtain the appropriate number of decomposition levels, the envelope spectrum is used to analyze the frequency composition of ZSV waveform illustrated in Fig. 4. The frequency band components of ZSV are calculated by the envelope spectrum, which is normalized and shown in Fig. 9.

When an SLG fault occurs, the main components of ZSV are concentrated in the low-frequency band, especially within 0-400Hz. In addition, intermittent faults are special cases in SLG faults, where multiple transient faults occur in a short period, so the ZSV in these cases has more high-frequency components [25]. The ZSV of an actual fault obtained from a substation and its normalized marginal spectrum is shown in Fig. 10.

Therefore, the ZSV is decomposed into four layers by Mallat algorithm. The approximate component $S_{2^4}^{(0)} f$ (0-312.5Hz) and the detailed component $W_{2^4}^{(3)} f$ (937.5-1250Hz) are taken as the analysis object of the fault diagnosis.

### B. Thresholds Calculation Method Based on Maximum Margin Hyperplane

Unbalanced line parameters may also cause ZSV to rise as mentioned previously. In general, if an SLG fault occurs, the ZSV will further increase, so the amplitude of the

ZSV between normal and SLG faults can be distinguished. Therefore, the appropriate threshold ε can be obtained by the maximum-margin hyperplane which is defined as **w**T · **x** + *b* = 0 [33], [34]. The distance from each input vector to the hyperplane can be expres

*yi*

×(**w**T·**x**i+)sedas*b*≥1,∀ *i*∈(1,2,...,*N*)(20)

where *yi* is the label of input vector, **x**i is the input vector, (×) represents performing a product operation, (·) represents performing a dot multiplication operation, **w** and *b* are the weight and bias, respectively. The following relationships can be satisfied.

{ T·,*y***wx** *i*+*b*=≥1 *i*=1

≤

{− (21)1,*yi*=−1 ∃ **w**T·**x**k1+*b*=1(**x**k1,**x**k2),*s.t.*

( **w**T· (22)**x**k2+*b*=−*b*=−**w**T·**x** T*k*1+**w**·) 1**x**k2/2 (23)

Construct all inputs into a one-dimensional array, the inputs with positive labels are *x*1, *x*2, . . . , *xm*, the inputs with negative labels are *xm* +1,*xm*+2,...,*xN*, *N* = *m* + *n*. Since the input one-dimensional variable, **w**T can be equivalent to *w*, and the following re

{lationshipcanbeobtained.*wxk*1=min(*wx*1,...,*wxm*)*wx*

*k*2 = (24)max(*wxm*+1,...,*wxm*+*n*)

To calculate the threshold, the expression of the maximum-margin hyperplane can be rewritten as

*w*ε1

+*b*=0 (25)

Based on (21)–(25), the threshold can be calculated.

ε1

=(min(*wx*1,...,*wx*)+···max(*wx*,...,*w*T*m m*+1 *xN*))/2*w*

(26)

Calculate *w* by the Lagrange multiplier method [34], the relevant expression is as follows.

1

// // *L*(*w*,*b*,λ)

// // // *w*2 // ∑*N*= + λ*i*(1−*yi*(*wxi*+*b*))2 *i*=1

{*s.t.*λ*i*≥0{(27)∂*L*(*w*,*b*,λ)*w*=∑0*w*0∂1λ*xy*∂(,,λ)→

∑−*Ni*=*iii*=*LwbNb*=(28)00∂*i*=1λ*iyi*=

The ZSV approximate components of unbalanced line parameters*S*(0)*f* (0)40bdandSLGfault*Sf*arebroughtinto(2 2 240*f* 6), the threshold can be calculated

ε

γ

= (0) (0)1(min(*wS*4*f*(*f*),...,*wS*4*f*210 2*m*(0*f*))+···

max(*wS*(0) *f*

+,...,*wS*(0)4*m*()4*fN*(0bd)2*w*(29)210bd))/2

### *C. Capture the Fault Occurrence Moment*

For the accurate extraction of fault transient features, it is very important to process the signals at the fault occurrence moment. Therefore, VMD-TEO algorithm is introduced to capture the fault occurrence moment. Where, VMD refers to an adaptive, non-recursive signal processing method [35], which can decompose the input signal *u* into multiple sub-signals with specific sparsity.

*k k* { ∑ )]min{*K*j−2*j*ω*t*,ω}*k*=1∂*t*∂(*t*)+π*tuk*(*t*)*e*2(31)

*u* *ku*

= ∑*u*}{[*s.tK.k*=

where δ(*t*) istheDiracfunction,*uk*isthedecomposedsignal,

ω*k* is the center frequency of each component. Obtaining the optimal solution of constraint expression by alternating direction multiplier method. TEO can quickly and accurately track the instantaneous changes of signal energy, which is defined as

[]d*st*2 d2[]=()−·*s*(*t*)ψ*s*(*t*) *s*(*t*) (32)dt d*t*2

where *s*(*t*) is the original signal. For discrete signals, the forward difference method is used to obtain the discrete expression of TEO.

ψ [*s*(*n*)]

=(*s*(*n*))2−*s*(*n*+1)×*s*(*n*−1) (33)

TEO of the first modal component is calculated, the moment when the first spike in the spectrum is located is the fault occurrence moment.

### *D. Judgment Method of SLG Fault Disappearance*

According to the waveform illustrated in Fig. 4, after the SLG fault disappears, ZSV starts to decrease, and its variation is large, which can be used as a criterion for detecting fault disappearance. However, when the fault resistance varies non-linearly, the ZSV also varies significantly. To distinguish the variation of ZSV is caused by fault disappearance or other disturbances, the approximate component variation and detailed component variation of ZSV are calculated.

The variations of approximate component and detailed component can be calculated by

{ *S* (*i*) = *S*(0) 24*f*(*i*) − *S*(0) 24*f*(*i* − *L*) ; *W* (*i*) = *W*(3)*f* 24(*i*) − *W*(3)*f*24(*i* − *L*) (34)

where *L* is the number of sampling points in a cycle.

Analyzing the field waveform of ZSV illustrated in Fig. 4, with the time window of 3s to 3.6s being intercepted. Its approximate component variation and detailed component variation are shown in Fig. 11(a). And Fig. 11(b) depicts the variation of approximate component and detailed component in the disturbance.

It can be seen that the detailed component is more sensitive to waveform change than the approximate component, the difference in approximate component variation between the fault disappearance and disturbance is more obvious. To distinguish

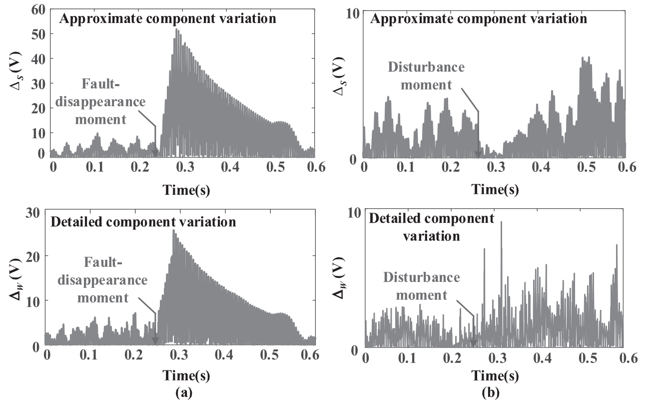


Fig.11. Approximate component variation and detailed component variation of ZSV: (a) SLG fault disappears, (b) SLG fault with disturbance.

TABLE II
CALCULATED FAULT THRESHOLDS

| Network configuration and fault conditions | | | Appropriate threshold (V) |
|---|---|---|---|
| Overcompensation of ASC (%) | Asymmetry of line (%) | Fault resistance(Ω) | |
| 5 | 1 | 1000 | 2590 |
| | | 3000 | [illegible] |
| | | 5000 | [illegible] |
| 5 | 0.5 | 3000 | [illegible] |
| | 1.5 | | [illegible] |
| | 2 | | [illegible] |
| 3 | 1 | 3000 | 1680 |
| 6 | | | 1440 |
| 9 | | | [illegible] |

from disturbance, the proposed maximum margin hyperplane is used to calculate the optimal threshold ε3 for detecting fault disappearance. If the approximate component variation exceeds ε3, it is considered that the SLG fault has disappeared.

In addition, according to Fig. 10, because of the short duration of intermittent faults, if the approximate component falls below the threshold ε1 or the detailed component falls below the threshold ε2, it also indicates that the fault has disappeared.

### *E. Online Calculated Method of the SLG Fault Thresholds*

According to Section II, the applicable fault threshold varies based on the different distribution network components, such as the asymmetry of line parameters, overcompensation of arc suppression coils, and fault resistance values. Although the optimal threshold can be calculated from the maximum margin hyperplane, the corresponding thresholds differ for distribution networks with different fault conditions. Based on the simulated data, the appropriate fault detection thresholds under different configurations and SLG fault conditions are presented in Table II.

Based on the analysis results of Section II-B, in case of low overcompensation of ASC and high asymmetry of line parameters, the amplitude of ZSV is high during normal operation of the distribution network, possibly exceeding the fault threshold associated with high overcompensation of ASC and low asymmetry of line parameters, leading to misjudgment of SLG faults. Therefore, the SLG fault detection thresholds should be calculated in real time. The comparison coefficient λ can be defined and used to avoid misjudgment caused by this situation:

$$\lambda = \frac{S_2^{(0)} f_{\text{train2}}}{S_2^{(0)} f_{\text{train1}}} \quad (35)$$

where $S_2^{(0)} f_{\text{train1}}$ is the approximate component under normal conditions in the training samples, $S_2^{(0)} f_{\text{train2}}$ is the approximate component under fault conditions in the training samples. The threshold-comparison coefficient $\varepsilon_\lambda$ between 1 and λ can be calculated by maximum margin hyperplane. Therefore, the fault threshold of approximate component ε1 can be expressed as

$$\varepsilon_1 = \varepsilon_\lambda \cdot \max\left(S_2^{(0)} f_{\text{test1}}\right) \quad (36)$$

where $\max(S_2^{(0)} f_{\text{test1}})$ is the approximate-component maximum value of ZSV collected in real time under normal condition. Similarly, ε2 can also be calculated. Additionally, ε3 is directly calculated based on the approximate component variation of ZSV through the maximum margin hyperplane.

### *F. SLG Fault Diagnosis Process*

The proposed fault diagnosis method can rapidly detect SLG faults, capture the fault occurrence moment, and estimate the fault nature. The flowchart for a fault diagnosis cycle is shown in Fig. 12. According to the IEEE standard 1234-2019 [36], the time criterion for the fault nature estimation is set to 10s. Consequently, the time for a fault diagnosis cycle is 10s. The specific steps are as follows.

Step 1: Collect ZSV signal in real time and calculate its approximate component $S_{24}^{(0)} f$ and detailed component $W_{24}^{(3)} f$.

Step 2: According to Section III-E, the fault-disappearance threshold ε3 can be calculated. And the SLG fault detection thresholds ε1 and ε2 are calculated in real time based on the sampled ZSV.

Step 3: An SLG fault occurs when the approximate or detailed component of ZSV exceeds the fault detection threshold ε1 or ε2. Meanwhile, the real-time calculation of these thresholds is stopped and the current thresholds are stored. And the fault occurrence moment is captured by the VMD-TEO algorithm.

Step 4: In the fault diagnosis cycle, if the fault does not satisfy the fault disappearance criterion, then the SLG fault is determined as the prolonged fault.

Step 5: The main characteristic of intermittent faults is that they occur several times in a short period and the duration is very short [37]. The transient faults exhibit longer fault durations than intermittent faults. Nevertheless, the transient faults disappear after a certain duration and are not characterized by recurrence. Therefore, in a fault diagnosis cycle, a fault is transient if it satisfies the fault disappearance criterion and does not recur. If it recurs more than three times, the fault is intermittent.

Step 6: The transient features are extracted based on the captured fault occurrence moment, which can be utilized to identify faulty feeder and faulty section.

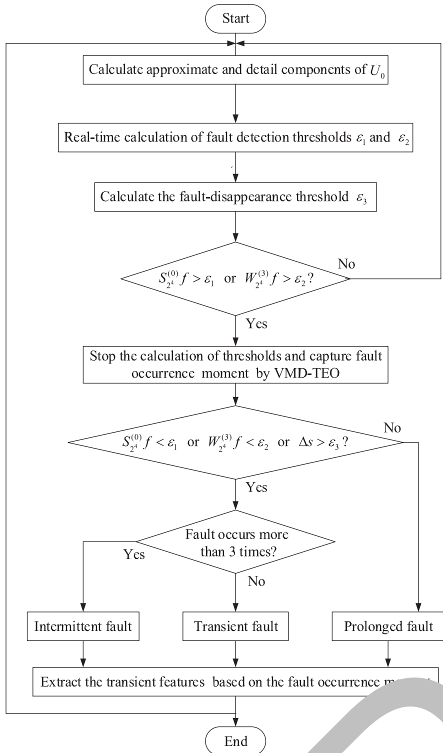


Fig. 12. SLG fault diagnosis flow chart.

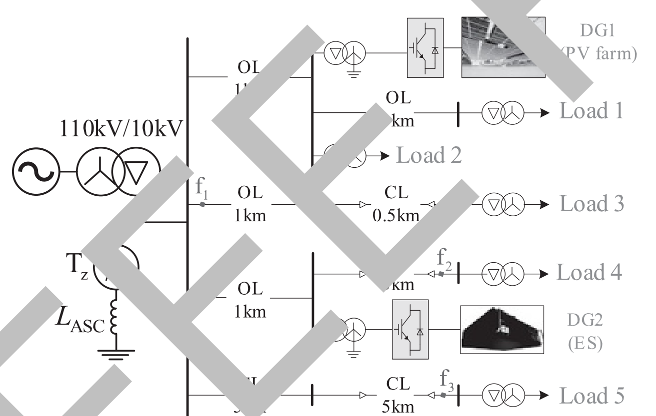


Fig.13. Simulationmodelof10kVactivedistributionnetwork,thepower supplies of DG1 and DG2 are 0.15MW and 0.1MW, respectively.

Step 7: After completing one cycle of fault diagnosis, the next cycle of diagnosis is started, realizing the online detection of SLG faults.

## IV. SIMULATIONVERIFICATION

The effectiveness of the proposed fault diagnosis method is verified by the 10kV active distribution network simulation model, which is shown in Fig. 13. Where $Tz$ is the grounding transformer, $f1$, $f2$, $f3$ are the fault points, OL is the overhead line, and CL is the cable line. Meanwhile, the IIDGs, such as photovoltaic (PV) farms and energy storage (ES) systems, are connected in the distribution network, which serves to verify the correctness of the analysis results in Section II-C.

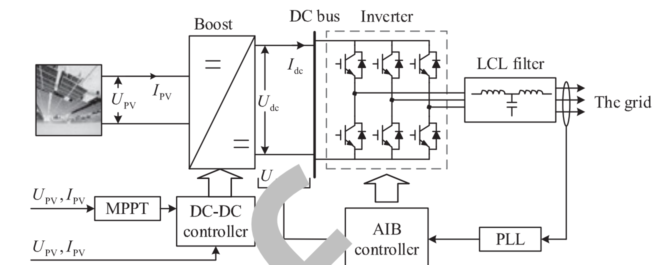


Fig. 14. The control block diagram of the PV system.

TABLE III
LINE DISTRIBUTION PARAMETER

| Line type | $r_0/r_1$(Ω/km) | $c_0/c_1$(μF/km) | $l_0/l_1$(mH/km) |
|---|---|---|---|
| OL | 0.2750/0.1250 | 0.0054/0.0096 | 4.6000/1.3000 |
| CL | [illegible] | 0.2800/0.3390 | 1.0190/0.2550 |

The control block diagram of the PV system is illustrated in Fig. 14. In the process of DC/DC control and inverter control, the adaptive integral backstepping (AIB) control scheme has high robustness [38]. Therefore, this non-linear controller is employed for the PV system.

Meanwhile, the ES system is connected to the grid through DC/AC converter, and can equivalently operate as an IIDG when it is in a power supply state [39], [40]. A basic two-level (2L) converter is employed as the converter within ES system, and its control strategy is droop control, which includes phase-locked loop (PLL) control, outer loop control, and inner loop control. The control block diagram of the 2L converter within the ES system is similar to that of the inverter utilized in the PV system [39].

The distribution lines adopt the pi-type equivalent model, the line distribution parameters are listed in Table III.

### A. SLG Fault Detection

*1) Calculate the SLG fault threshold:* In the distribution network, the asymmetry of OL parameters is typically within 1.5% and the asymmetry of CL parameters is typically within 0.5% [41]. The model shown in Fig. 13 has been simulated with the ASC overcompensation of 2-10% with a step of 2%, and the fault resistances of 10 , 50 , 500 , and 5000 . From the simulation, 30 sets of data representing normal operating conditions and their corresponding 120 sets of data representing SLG fault conditions can be obtained. The relative threshold ελ can be calculated as 2.7 by the maximum margin hyperplane.

The Mallat algorithm can quickly decompose the original signal, which only requires 46 sample points of discrete data, this process takes only 4.6ms with a sample rate of 10kHz. Therefore, the fault thresholds can be calculated quickly.

However, if the line parameters and the loads are symmetrical, the ZSV under normal conditions is relatively low, which can lead to the fault thresholds being small, thus resulting in the fault detection algorithm being too sensitive. Therefore, a reference value of approximate component $S(0)$ 24 $f$ref is set to improve the robustness of fault detection algorithms. The

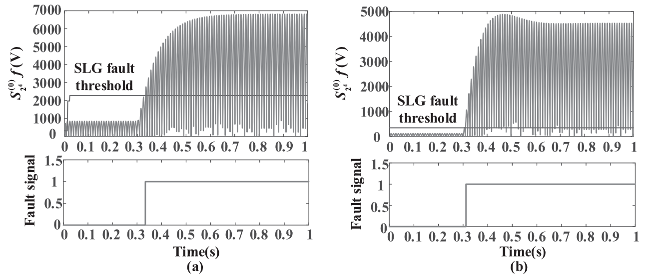


Fig.15. The detection results of SLG fault: (a) Approximate component exceeds $S_{24}^{(0)} f_{ref}$ under normal conditions, (b) Approximate component does not exceed $S_{24}^{(0)} f_{ref}$ under normal conditions.

TABLE IV
THE ANALYSIS RESULTS OF FAULT DETECTION

| Line type | Overcompensa-tion of ASC | Asymmetry | Fault resistance (Ω) | Number of cases | Correct rate |
|---|---|---|---|---|---|
| OL | 2% - 10% | 0.5% - 1.5% | 10, 50, 500,5000 | 25 | 100% |
| CL | 2% - 10% | 0.2% - 0.5% | | 30 | 100% |

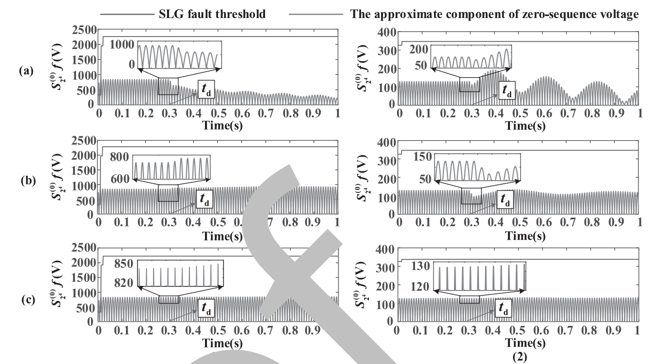


Fig.16. The detection results of non-fault disturbances: (a) CS, (b) LS, (c) DGO, and (1) Approximate component exceeds $S_{24}^{(0)} f_{ref}$ under normal conditions, (2) Approximate component does not exceed $S_{24}^{(0)} f_{ref}$ under normal conditions.

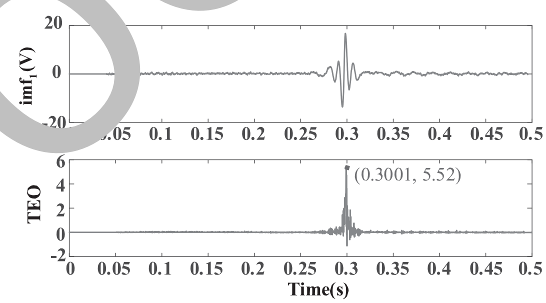


Fig. 17. The waveforms of the first modal component and its TEO.

following relationship should be satisfied.

$$\varepsilon_1 = \begin{cases} \lambda \cdot (\max S_{24}^{(0)} f_1), & \max(S_{24}^{(0)} f_1) \geq S_{24}^{(0)} f_{ref} \\ \lambda \cdot S_{24}^{(0)} f_{ref}, & \max(S_{24}^{(0)} f_1) < S_{24}^{(0)} f_{ref} \end{cases} \quad (37)$$

Consider the ZSV of a normally operating neutral ungrounded system under the condition of maximum line parameter imbalance, $S_{24}^{(0)} f_{ref}$ can be calculated as 120V.

2) *Analysis of simulation results of SLG faults:* Because the Mallat algorithm simplifies the signal decomposition process, thresholds under normal system conditions can be quickly calculated. Take the cases where approximate components exceed $S_{24}^{(0)} f_{ref}$ and those do not exceed $S_{24}^{(0)} f_{ref}$ under normal conditions as examples, the fault detection results are illustrated in Fig. 15.

The rate of correct SLG fault detection under different situations is shown in Table IV.

3) *Influence of non-fault disturbances:* The non-fault disturbances discussed in this paper include load switching (LS), capacitor switching (CS), and DG off-grid (DGO) [42]. In Fig. 16, $t_d$ is the occurrence moment of disturbance, the detection results of these three non-fault disturbances are demonstrated. It can be observed that the approximate components of non-fault disturbances do not exceed the SLG fault threshold. For LS and CS, the change in ZSV is due to a surge in the transient switch. Meanwhile, because the line parameters are asymmetrical, after the switching action, the ZSV will oscillate. Because the amplitude of this oscillation is attenuated, the ZSV does not exceed the threshold which is calculated in real time. In addition, because the primary sides of DG transformers are delta connected and not grounded [13], when the DGs are disconnected, the ZSV does not change significantly.

### B. Capture the Occurrence Moment of SLG Fault

In resonant ground systems, there is a time interval between the fault detected moment and the actual fault occurrence moment. The higher the fault resistance, the longer this time interval will be. Part of the difficulty in detecting HIFs is due to inaccurate estimation of fault occurrence moment. In this paper, the VMD-TEO algorithm is utilized to capture the SLG fault occurrence moment. The simulation data collected from the distribution network depicted in Fig. 13 is utilized as the example, a time window with a length of 0.5s is chosen, assuming the SLG fault occurs at 0.3s and the fault resistance is 2000 . Meanwhile, the Gaussian white noise is added to ZSV with a signal-to-noise ratio of 5dB. After the 5-layer decomposition of ZSV by utilizing VMD, the waveforms of the first modal component (imf1) and its TEO are shown in Fig. 17.

It can be observed that the estimation error of detected fault occurrence moment is only 0.1ms. Taking into account the potential for extreme fault scenarios in actual distribution networks, noise above 2000Hz is filtered out during the data processing stage to enhance the robustness of the proposed fault diagnosis method.

### C. SLG Fault Nature Estimate

According to the requirements of the relay protection system, the accurate estimation of SLG fault nature is important. The simulation obtained 150 sets of ZSV data with transient, intermittent and permanent fault, which include

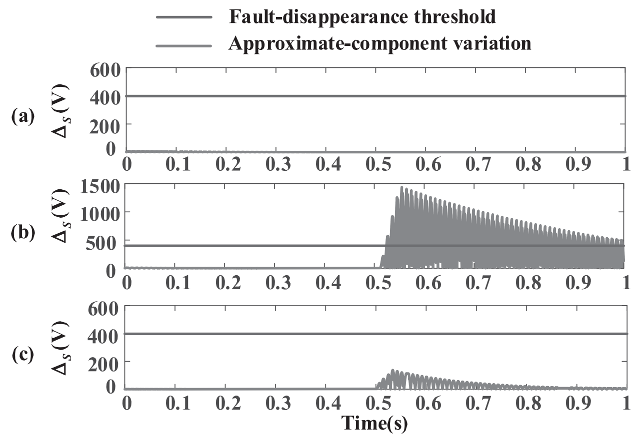


Fig.18. SLGfaultdisappearancejudgment:(a)Prolongedfault,(b)Transient fault, (c) Fault resistance variation.

TABLEV
FAU LTOCCURRENCE ANALYSIS RESULTS

| Inception angle(°) | Fault resistance(Ω) | $\eta_1$ | $\eta_2$ | $t_1$ (s) | $t_2$ (s) |
|---|---|---|---|---|---|
| ≤ 45 | ≤ 2000 | 100% | 100% | 0.0[illegible] | [illegible]0002 |
| | >2000 | 100% | 100% | [illegible]79 | [illegible]003 |
| >45 | ≤ 2000 | 100% | 100% | 0.019 | 0.[illegible]01 |
| | >2000 | 100% | 100% | 0.023 | 0.[illegible]01 |

" $\eta_1$ " means the rate of correct fault detection, " $\eta_2$ " [illegible]ns the r[illegible] of correct fault disappearance detection, " $t_1$ " means the maximum [illegible]rval between the fault detected moment and the actual fault occurrence mo[illegible]. " $t_2$ " means the maximum error of fault occurr[illegible] moment.

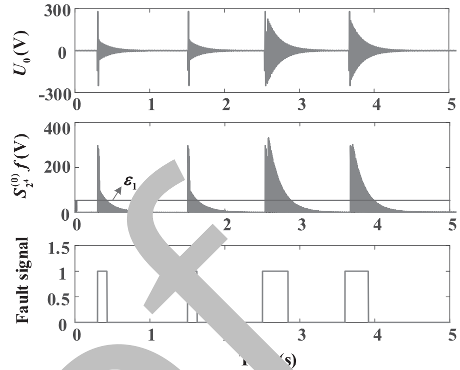


Fig.19. Intermittentfaultdetectionanalysis:(a)ZSV,(b)Theapproximate component, (c) The fault signal.

TABLE VI
THERESULTS OF SENSITIVITY ANALYSIS

| Fault position | $\eta_1$ | $\eta_2$ | $t_2$ (s) |
|---|---|---|---|
| $f_1$ | 100% | 100% | 0.002 |
| [illegible] | 100% | 100% | 0.006 |

### D. Sensitivity Analyses of the Proposed Method

The impedance of the line leads to a certain voltage, which can usually be ignored. It is defined as the distribution line voltage in this paper. Without considering the distribution line voltage, the ZSV measured at different positions is consistent. However, when the line is very long, the influence of the distribution line voltage on ZSV at different measurement

different fault resistances, different line parameters asymmetry, positions along this line cannot be ignored.
and different arc suppression coil overcompensation degrees. Furthermore, when the HIF occurs, the small amplitude Then, the threshold for fault disappearance is calculated as of ZSV and the long transient process are challenging for 398V by the maximum margin hyperplane. The distinguished SLG fault diagnosis. Therefore, it is necessary to analyze the results between prolonged faults and transient faults are shown applicability of the proposed fault diagnosis method in these inFig.18. cases.
Only when the SLG fault disappears, the approximate- According to Fig. 13, it is assumed that the SLG fault
component variation of ZSV will exceed the fault occursatthebeginningofashortline$f$1 ortheendofa
disappearance threshold. Through the active distribution long line f3, with fault resistances of 10k , 13k , 16k ,
network model illustrated in Fig. 13, the cases of different and fault inception angles of 0∘, 30∘, 60∘, 90∘, respectively. fault resistances and different line asymmetry are simulated, The overcompensation of ASC is 5% and 10%, respectively. and the fault diagnosis results are shown in Table V. It can And the asymmetry degree of the line parameters is 1%.
be observed that the proposed fault diagnosis method can Consequently, there are 24 sets of fault samples for both $f$1
accurately detect the occurrence and disappearance of SLG and f3. Assuming a perfect instrument transformer is used,
faults, and accurately capture the fault occurrence moment. measurement errors can be disregarded, the test results are
According to the analysis of intermittent faults, if an SLG shown in Table VI.
fault occurs and disappears more than three times within 10s, It can be observed that the proposed fault diagnosis method it can be judged as intermittent fault. Under the condition of still can reliably detect the occurrence and disappearance of intermittent faults, if the approximate component falls below SLG faults. However, when the fault occurs at the end of the
the threshold ε1 or the detailed component falls below the long line and the fault resistance is high, the estimation results
threshold ε2, it indicates that the fault has disappeared. Take of the fault occurrence moment have a relatively large error.
the approximate component as an illustrative example. The That is because the ZSV amplitude of a HIF is relatively low. It characteristics of the intermittent faults and the detection result is difficult to accurately detect the small changes in the ZSV if andareshowninFig.19. themeasurementpositionisfarfromthefaultpoint.InFig.20, It can be observed from Fig. 19(c) that the proposed method a violin plot is utilized to illustrate the estimation error of fault effectively detects the occurrence and disappearance of SLG occurrence moment, which includes 288 sets of simulation faults, which ensures the reliable identification of intermittent data. The median estimation error of fault occurrence moment SLGfaults.
is0.1ms.Themaximumpositiveerrorandminimumnegative

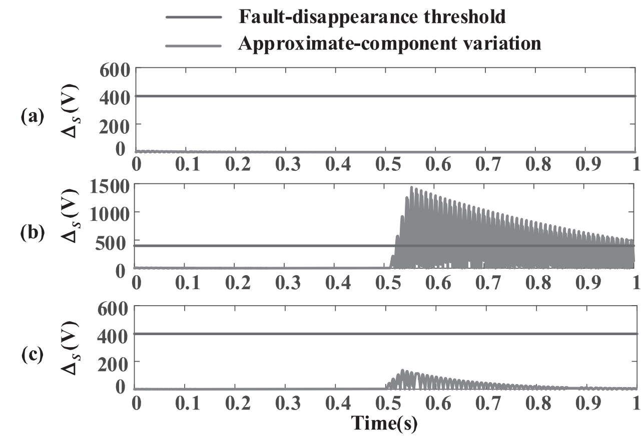


Fig. 20. The error of fault occurrence moment for the proposed method.

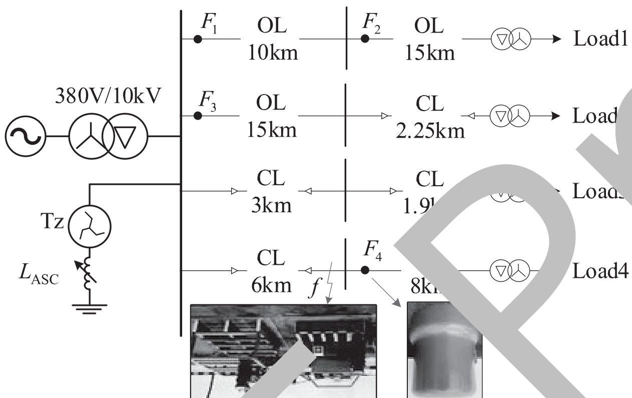


Fig. 21. Power distribution network experimental structure.

error are 6ms and -3.6ms, respectively. It can be observed that the proposed method provides a relatively accurate estimation of fault occurrence moment.

In addition, to mitigate the influence of long distribution lines on the precision of fault occurrence moment estimation, the algorithms introduced in this paper are integrated within FTUs of overhead lines. Consequently, several measurement points are configured in the distribution network so that the fault position and the measurement position are as close as possible.

## V. EXPERIMENTAL AND FIELD VALIDATION

### A. Experimental Platform and Data Analysis

The effectiveness of the proposed fault diagnosis method is further verified by the 10kV distribution network prototype experimental platform. The structure of this experimental system is shown in Fig. 21, where *Fi*, *i* =1,2,...,4,indicates the installation position of the FTUs. The line parameters are shown in Table VII.

Through this experimental platform, the conditions of resistance grounding fault, stone grounding fault and branches grounding fault are simulated. Among them, the fault resistances of resistance grounding faults are 100 , 200 , 2000 , 5000 , 10k , and 16k , respectively, including the simulation of HIFs. The 10kV prototype experimental platform is shown in Fig. 22, which includes four feeders and simulated fault scenarios. These feeders are simulated through Pi RL components. In Fig. 22, ZT is the grounding transformer, DR is the damping resistance, RT is the regulator transformer, and ST is the step-up transformer. The designed FTU and its connection method are shown in Fig. 23. The fault diagnosis algorithm is embedded in the Raspberry Pi of the designed FTU. The ZSV is collected and stored by the AD7606 chip and STM32F407 microcontroller and then sent to the Raspberry Pi which has two processes running the fault detection algorithm and the fault occurrence moment capture algorithm respectively. When the microcontroller has stored a 0.5s length of ZSV, it is sent to the Raspberry Pi and starts the next 0.5s acquisition. In addition, the SLG fault detection algorithm calculates the fault threshold in real time and it takes only 0.038s to judge whether the fault occurs. If an SLG fault occurs, it stops the threshold calculation and saves the current thresholds, and then sends the ZSV data for the first 0.2s and the last 0.1s of that detection point to the fault occurrence moment capture algorithm. It takes only 0.12s to calculate the fault occurrence moment. Therefore, the real-time diagnosis of SLG faults can be realized.

The branches grounding faults are usually accompanied by fault arcing and have the characteristics of HIFs. The burning of branches and changes in arc length usually result in unstable fault resistance. Therefore, to better illustrate the effectiveness of the proposed fault diagnosis method, take the branches grounding fault as an example. The detection results of SLG fault occurrence and disappearance are shown in Fig. 24. When the fault signal is 1, it indicates that an SLG fault has occurred. When the fault signal is 0, it indicates

TABLE VII
SIMULATED LINE PARAMETERS

| Line number | Line type | Capacitive current(A) | Simulated length(km) | Total capacitance($\mu$F) |
|---|---|---|---|---|
| 1 | OL | 3.4 | 25 | 10.8 |
| 2 | OL&CL | 8 | 17.35 | |
| 3 | CL | 10 | 4.9 | |
| 4 | CL | 20 | 9.7 | |

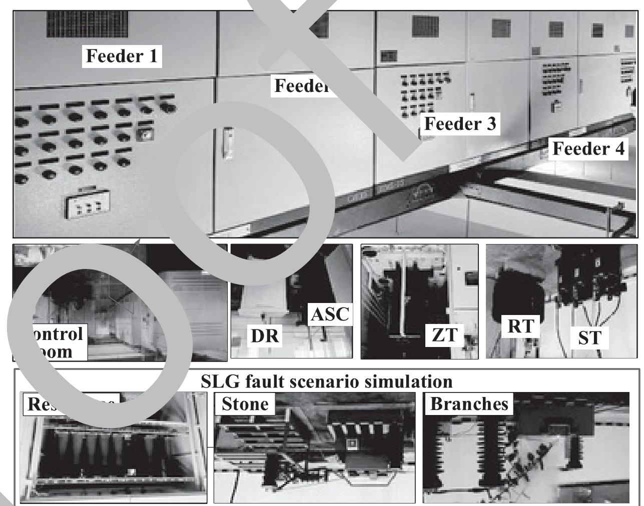


Fig. 22. 10kV experimental platform and the simulated SLG fault scenarios.

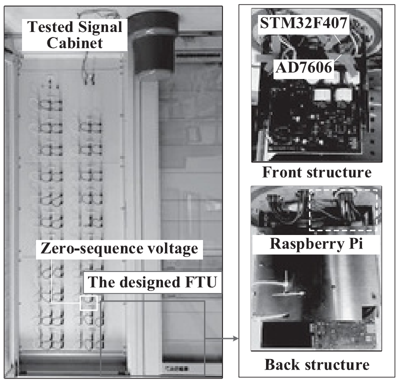


Fig. 23. The designed FTU and the exhibition of its connection method.

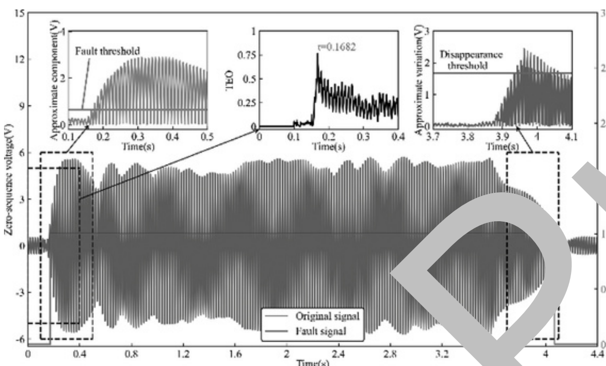


Fig. 24. Experimental data analysis.

TABLE VIII
EXPERIMENTAL DATA ANALYSIS RESULTS

| Fault scenarios | Number of cases | $\eta_1$ | $\eta_2$ | $t_2$ (s) |
|---|---|---|---|---|
| Resistance grounding | 54 | [illegible] | 100% | 0.0030 |
| Stone grounding | 21 | 100% | 100% | 0.0005 |
| Branches grounding | 24 | 100% | 100% | 0.0012 |

"$t_2$" means the maximum error to capture the moment of fault.

that the fault disappears. Furthermore, the proposed fault diagnosis method can capture the fault occurrence moment. Table VIII shows the detection results of different fault scenarios.

Several non-fault disturbances are simulated on the experimental platform to verify the robustness of the proposed method, including transformer energization, cold load pickup, hot load removal, and rotating load connection. Among them, the cold load pickup is simulated by connecting the load of Feeder 2, which is initially in a non-operational state, during the normal operation of the experimental system. And the hot load removal is simulated by subsequently removing the load of Feeder 2 after the experimental system has operated with this load for 15 hours. Taking the approximate component of ZSV as an example, the detection results of these non-fault disturbances are shown in Fig. 25. It can be observed that these non-fault disturbances will not be misclassified as SLG faults.

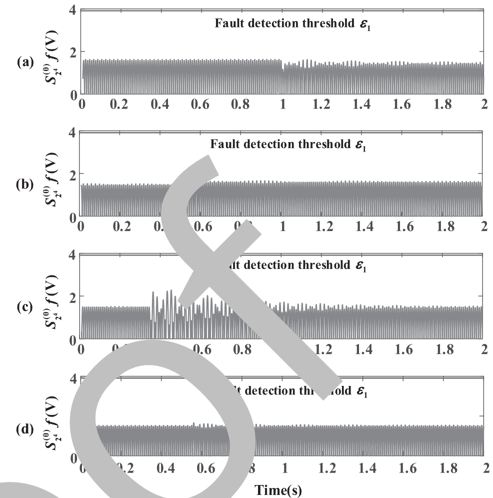


Fig.25. The approximate component of ZSV: (a) Transformer energization, (b) Cold load pickup, (c) Hot load removal, (d) Rotating load connection.

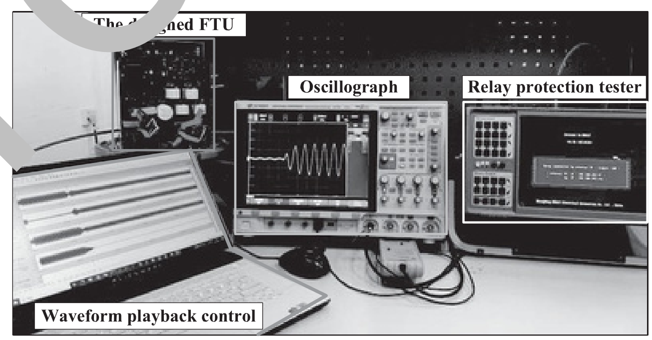


Fig. 26. The field data playback.

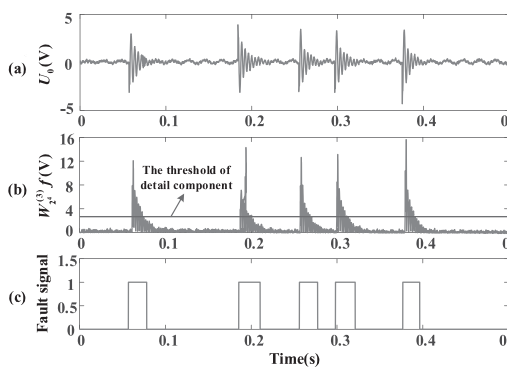


Fig.27. Intermittent fault detection analysis: (a) Original signal, (b) The detailed component of ZSV, (c) Fault signal.

## B. Field Data Analysis

Through the relay protection tester, the fault record data in the actual distribution network can be reproduced. The waveform testing for the actual distribution network is depicted in Fig. 26. Taking the fault data of a master station as an example, the test results of the fault occurrence and disappearance are illustrated in Fig. 27. It can be observed that the SLG fault repeatedly occurs 5 times in a short period. Therefore, it is the data of intermittent fault. Table IX shows the analysis results of

TABLE IX
FIELD DATA ANALYSIS RESULTS

| Fault type | Number of cases | $\eta_1$ | $\eta_2$ | $\eta_3$ | $t_2$ (s) |
|---|---|---|---|---|---|
| Intermittent fault | 5 | 100% | 100% | 100% | 0 |
| Transient fault | 19 | 100% | 94.74% | 94.74% | 0.0010 |
| Prolonged fault | 15 | 93.33% | 100% | 93.33% | 0.0002 |

" $\eta_3$ " means the rate of correct fault nature estimation.

TABLE X
RESULTS OF THE COMPARISON

| Method | $\eta_1$ | $\eta_4$ | $t_2$(s) |
|---|---|---|---|
| TFD | 72.46% | 82% | 0.038 |
| EWT-DFE | 94.92% | 94% | 0.029 |
| MM | 79.71% | 56% | 0.010 |
| DWT | 91.30% | 60% | 0.008 |
| The proposed method | 99.27% | 98% | 0.002 |

the field data which is measured from an operating distribution system.

It can be observed that the feasibility and effectiveness of the proposed fault diagnosis method have been verified.

### C. Comparison and Analysis

The effectiveness of different methods for SLG fault diagnosis is compared by the experimental data and field data. The criterion for traditional fault detection methods (TFD) is whether the ZSV exceeds 15% of the phase voltage [11]. In [13], a fault detection method based on empirical wavelet transform and differential faulty energy (EWT-DFE) is proposed. In [17], mathematical morphology (MM)-based method is utilized to detect SLG faults. And a discrete wavelet transform (DWT)-based fault detection method is proposed in [25]. Through the experimental data and field data, fault detection correct rate $\eta_1$, non-fault disturbance detection correct rate $\eta_4$, and maximum error for fault occurrence moment $t_2$ of these methods and the proposed method are calculated and listed in Table X. There are 138 sets of SLG fault data, and 50 sets of non-fault disturbance data, including CS, LS and transformer energization, etc.

It can be observed that the proposed fault diagnosis method exhibits the highest correct rate in fault detection as well as non-fault disturbance detection. Although EWT-DFE-based method also achieves high correct rate, it does not provide an estimation of the fault occurrence moment. Consequently, the error of fault occurrence moment is relatively large. In a resonant ground system, if the faulty feeder and section identification algorithms have not been triggered within one cycle after the occurrence of an SLG fault, the feature difference between the healthy and faulty feeders may decrease. Therefore, the minor error in fault occurrence moment can contribute to enhancing the rate of correct faulty feeder and faulty section identification.

In addition, the fault diagnosis thresholds of the proposed method are calculated in real time through the maximum margin hyperplane and can be better adapted to different asymmetric conditions of the distribution network. Meanwhile, the proposed method also integrates three functions, namely fault detection, fault occurrence moment capture and fault nature estimation, improving the utilization rate of the designed device.

## VI. CONCLUSION

This paper has proposed an SLG fault diagnosis method for resonant ground systems. Firstly, the ZSV is collected by FTU. Then, the approximate and detailed components are calculated and compared separately with their thresholds which are the optimal thresholds calculated by the maximum margin hyperplane in real time. Finally, effective fault detection and accurate fault nature estimation have been realized. The following key conclusions can be obtained from this research work:

1) The proposed fault diagnosis method calculates the SLG fault thresholds in real time, which makes the method highly robust to line parameter imbalance and non-fault disturbances. Its feasibility and applicability are verified by simulation, experimental and field data.

2) The proposed fault diagnosis method has the capability of accurately capturing the moment of fault occurrence, which has been verified. It is of great importance in accurately extracting the transient features of SLG faults and improving the accuracy of faulty feeder and faulty section identification.

3) This method integrates the three functions of fault detection, fault occurrence moment capture and fault nature estimation with the same requirements for hardware devices and measurement signals, which improves the applicability and equipment utilization of the designed FTU.

## REFERENCES

[1] "IEEE PES distribution system analysis subcommittee." Distribution Test Feeders. 2017. [Online]. Available: http://ewh.ieee.org/soc/ pes /dsacomtestfeeders/index.html
[2] H. L. Willis, "Power delivery systems," in *Power Distribution Planning Reference Book*, 2nd ed. Boca Raton, FL, USA: CRC Press, 2004, pp. 29–35, ch. 1.
[3] Y.Duetal.,"Singleline-to-groundfaultedlinedetectionofdistribution systems with resonant grounding based on feature fusion framework," *IEEE Trans. Power Del.*, vol. 34, no. 4, pp. 1766–1775, Aug. 2019.
[4] M.A.Barik,A.Gargoom,M.A.Mahmud,M.E.Haque,H.Al-Khalidi, and A. M. Than Oo, "A decentralized fault detection technique for detecting single phase to ground faults in power distribution systems with resonant grounding," *IEEE Trans. Power Del.*, vol. 33, no. 5, pp. 2462–2473, Oct. 2018.
[5] J. Li, Y. Liu, C. Li, D. Zeng, H. Li, and G. Wang, "An FTU-based method for locating single-phase high-impedance faults using transient zero-sequence admittance in resonant grounding systems," *IEEE Trans. Power Del.*, vol. 37, no. 2, pp. 913–922, Apr. 2022.
[6] C.Ozansoy,"Performanceanalysisofskewnessmethodsforasymmetry detection in high impedance faults," *IEEE Trans. Power Syst.*, vol. 35, no. 6, pp. 4952–4955, Nov. 2020.
[7] S.-R. Nam, S.-H. Kang, S.-J. Ahn, and J.-H. Choi, "Single line-to-ground fault location based on unsynchronized phasors in automated ungrounded distribution systems," *Electr. Power Syst. Res.*, vol. 86, pp. 151–157, May 2012.
[8] D. R. R. Penido, L. R. De Araujo, V. T. S. Rodrigues, and K. B. Do Nascimento, "An analytical zero sequence method to locate fault in distribution systems rich in DG," *IEEE Trans. Smart Grid*, vol. 13, no. 3, pp. 1849–1859, May 2022.
[9] Y. Zhang, S. Xie, and S. Shu, "Decentralized optimization of multi-area interconnected traffic-power systems with wind power uncertainty," *IEEE Trans. Ind. Info.*, vol. 19, no. 1, pp. 133–143, Jan. 2023, doi: 10.1109/TII.2022.31528-15.

[10] *Microgrid Protection Systems*, IEEE Power Energy Soc., Piscataway, NJ, USA, Jul. 2019.

[11] X.Wangetal.,“Locationofsinglephasetogroundfaultsindistribution networks based on synchronous transients energy analysis,” *IEEE Trans. Smart Grid*, vol. 11, no. 1, pp. 774–785, Jan. 2020.

[12] A. N. Milioudis, G. T. Andreou, and D. P. Labridis, “Enhanced protection scheme for smart grids using power line communications techniques—Part-II: Location of high impedance fault position,” *IEEE Trans. Smart Grid*, vol. 3, no. 4, pp. 1631–1640, Dec. 2012.

AQ2 [13] J. Gao, X. Wang, X. Wang, A. Yang, H. Yuan, and X. Wei, “A high-impedance fault detection method for distribution systems based on empirical wavelet transform and differential faulty energy,” *IEEE Trans. Smart Grid*, vol. 13, no. 2, pp. 900–912, Mar. 2022.

[14] Z. Y. Zheng, M. F. Guo, N. C. Yang, and T. Jin, “Single-phase flexible arc suppression device based on BSC-SOGI-PLL method for distribution networks,” *Int. J. Electr. Power Energy Syst.*, vol. 121, Oct. 2020, Art. no. 106100.

[15] M. F. Guo, X. D. Zeng, D. Y. Chen, and N. C. Yang, “Deep-learning-based earth fault detection using continuous wavelet transform and convolutional neural network in resonant grounding distribution systems,” *IEEE Sensors J.*, vol.18, no.3, pp.1291–1300, Feb. 2018.

[16] K. Sarwagya, S. De, and P. K. Nayak, “High-impedance fault detection in electrical power distribution systems using moving sum approach,” *IET Sci. Meas. Technol.*, vol. 12, no. 1, pp. 1–8, Jan. 2018.

[17] S. Gautam and S. M. Brahma, “Detection of high impedance fault in power distribution systems using mathematical morphology,” *IEEE Trans. Power Syst.*, vol. 28, no. 2, pp. 1226–1234, May 2013.

[18] A. N. Milioudis, G. T. Andreou, and D. P. Labridis, “Detection and location of high impedance faults in multiconductor overhead distribution lines using power line communication devices,” *IEEE Trans. Smart Grid*, vol. 6, no. 2, pp. 894–902, Mar. 2015.

[19] E.M.Limaetal.,“Highimpedancefaultdetectionmethodbasedonthe short-time Fourier transform,” *IET Gener., Transmiss. Distrib.*, vol. 12, no. 11, pp. 2577–2584. Apr. 2018.

[20] D. Li, A. Ukil, K. Satpathi, and Y. M. Yeap, “Hilbert–Huang transform based transient analysis in voltage source converter interfaced direct current system,” *IEEE Trans. Ind. Electr.*, vol. 68, no. 11, pp. 11014–11025, Nov. 2021.

[21] M. F. Guo, N. C. Yang, and L. X. You, “Wavelet-transform based early detection method for short-circuit faults in power distribution networks,” *Int. J. Elect. Power Energy Syst.*, vol. 99, pp. 706–721, Jul. 2018.

[22] X. Chen, “Real wavelet transform-based phase information extraction method: Theory and demonstrations,” *IEEE Trans. Ind. Electr.*, vol. 56, no. 3, pp. 891–899, Mar. 2009.

[23] X. Wang et al., “High impedance fault detection method based on variational mode decomposition and Teager–Kaiser energy operators for distribution network,” *IEEE Trans. Smart Grid*, vol. 10, no. 6, pp. 6041–6054, Nov. 2019.

[24] D. A. Gadanayak and R. K. Mallick, “Interharmonics based high impedance fault detection in distribution systems using maximum overlap wavelet packet transform and a modified empirical mode decomposition,” *Int. J. Elect. Power Energy Syst.*, vol. 112, pp. 282–293, Nov. 2019.

[25] C. Lin, W. Gao, and M. F. Guo, “Discrete wavelet transform-based triggering method for single-phase earth fault in power distribution systems,” *IEEE Trans. Power Del.*, vol. 34, no. 5, pp. 2058–2068, Oct. 2019.

[26] Y. Liang, K.-J. Li, Z. Ma, and W.-J. Lee, “Multilabel classification model for type recognition of single-phase-to-ground fault based on KNN-Bayesian method,” *IEEE Trans. Ind. Appl.*, vol. 57, no. 2, pp. 1294–1302, Mar./Apr. 2021.

[27] X. Liang, S. A. Wallace, and D. Nguyen, “Rule-based data-driven analytics for wide-area fault detection using synchrophasor data,” *IEEE Trans. Ind. Appl.*, vol. 53, no. 3, pp. 1789–1798, May 2017.

[28] Q. Cui and Y. Weng, “Enhance high impedance fault detection and location accuracy via μ-PMUs,” *IEEE Trans. Smart Grid*, vol. 11, no. 1, pp. 797–809, Jan. 2020.

[29] J. Fang, Y. Yan, H. Zhang, H. Wang, and Y. Wang, “Research on fault section location method of distribution networks with arc suppression coil grounding based on energy leakage function,” *IET Gener. Transm. Distrib.*,vol. 14, no.25, pp. 6097–6106, Dec. 2020.

[30] J. Yuan, Y. Hu, Y. Liang, and Z. Jiao, “Faulty feeder detection for single line-to-ground fault in distribution networks with DGs based on correlation analysis and harmonics energy,” *IEEE Trans. Power Del.*, vol. 38, no. 2, pp. 1020–1029, Apr. 2023.

[31] Z. Shuai, C. Shen, X. Yin, X. Liu, and Z. J. Shen, “Fault analysis of inverter-interfaced distributed generators with different control schemes,” *IEEE Trans. Power Del.*, vol. 33, no. 3, pp. 1223–1235, Jun. 2018.

[32] W.-M. Guo, L.-H. Mu, and X. Zhang, “Fault models of inverter-interfaced distributed generators within a low-voltage microgrid,” *IEEE Trans. Power Del.*, vol. 32, no. 1, pp. 453–461, Feb. 2017.

[33] R. Jiang and Y. Zheng, “Series arc fault detection using regular signals and time-series reconstruction,” *IEEE Trans. Ind. Electr.*, vol. 70, no. 2, pp. 2026–2036, Feb. 2023.

[34] J. C. Burges, “A tutorial on support vector machine for pattern recognition, *Data Min. Knowl. Discovery*, vol. 2, no. 2, pp. 121–167, Jun. 1998.

[35] L. Xie, L. Luo, Y. Li, Y. Zhang, and Y. Cao, “A traveling wave-based fault location method employing VMD-TEO for distribution network,” *IEEE Trans. Power Del.*, vol. 35, no. 4, pp. 1987–1998, Aug. 2020.

[36] *IEEE Guide for Fault Locating Techniques on Shielded Power Cable Systems*, IEEE Standard 1234-2019, Jun. 12, 2019.

[37] M. M. Alamuti, H. Nouri, R. M. Ciric, and V. Terzija, “Intermittent fault location in distribution feeders,” *IEEE Trans. Power Del.*, vol. 27, no. 1, pp. 96–103, Jan. 2012.

[38] M. M. Rahman, S. P. Biswas, M. R. Islam, M. A. Rahman, and K. M. Muttaqi, “An advanced nonlinear controller for the LCL-type three-phase grid-connected solar photovoltaic system with a DC–DC converter,” *IEEE Syst. J.*, vol. 16, no. 2, pp. 3203–3214, Jun. 2022.

[39] G. Wang et al., “A review of power electronics for grid connection of utility-scale battery energy storage systems,” *IEEE Trans. Sustain. Energy*, vol. 7, no. 4, pp. 1778–1790, Oct. 2016.

[40] G. G. Farivar et al., “Grid-connected energy storage systems: State-of-the-art and emerging technologies,” *Proc. IEEE*, vol. 111, no. 4, pp. 397–420, Apr. 2023.

[41] W. Wang, X. Gao, B. Fan, X. Zeng, and G. Yao, “Faulty phase detection method under single-line-to-ground fault considering distributed parameters asymmetry and line impedance in distribution networks,” *IEEE Trans. Power Del.*, vol. 37, no. 3, pp. 1513–1522, Jun. 2022.

[42] W.H.Kwon,G.W.Lee,Y.M.Park,M.C.Yoon,andM.H.Yoo,“High impedance fault detection utilizing incremental variance of normalized even order harmonic power,” *IEEE Trans. Power Del.*, vol. 6, no. 2, pp. 557–564, Apr. 1991.


**Jiahao Lin** (Student member, IEEE) was born in Fujian, China, in 1997. He received the B.S. degree in electric machines and electric apparatus from Fuzhou University, Fujian, in 2019, where he is currently pursuing the Ph.D. degree. His main research interest is the detection and location of single-line-to-ground fault in distribution network.

**Moufa Guo** (Member, IEEE) was born in Fujian, China, in 1973. He received the B.S. and M.S. degrees in electrical engineering from Fuzhou University, Fuzhou, China, in 1996 and 1999, respectively, and the Ph.D. degree in electrical engineering from Yuan Ze University, Taoyuan, Taiwan, in 2018.

Since 2000, he has been with Fuzhou University, where he is currently a Professor with the College of Electrical Engineering and Automation. His research interests include the information processing, protection control, and flexible arc suppression of single-line-to-ground fault in distribution networks.

**Qiteng Hong** (Senior Member, IEEE) received the B.Eng. (Hons.) and Ph.D. degrees in electronic and electrical engineering from the University of Strathclyde, Glasgow, U.K., in 2011 and 2015, respectively, where he is currently a Senior Lecturer (Associate Professor). His main research interest is on power system protection and control in future networks with high penetration of renewables. He is a member of IEEE Working Group P2004 and IEEE Task force on Cloud-Based Control and Co-Simulation of Multi-Party Resources in Energy Internet, and he also was a Regular Member of the completed CIGRE WG B5.50.

**Run Jiang** (Student Member, IEEE) received the B.S. and M.S. degrees from Fuzhou University, Fujian, China, in 2016 and 2020, respectively. He is currently pursuing the Ph.D. degrees in electrical engineering with Fuzhou University and Yuan Ze University, Taoyuan, Taiwan. His main research interests include measurement technology on fiber-optic current sensing, arc model, and AC/DC series arc fault detection.